Angewandte Chemie
Eine Zeitschrift der Gesellschaft Deutscher Chemiker

Supporting Information

Allosteric Recognition of Homomeric and Heteromeric Pairs of Monosaccharides by a Foldamer Capsule

Pedro Mateus, Nagula Chandramouli, Cameron D. Mackereth, Brice Kauffmann, Yann Ferrand, and Ivan Huc**

ange_201914929_sm_miscellaneous_information.pdf

This PDF file includes:

1. Methods for NMR, Circular Dichroism and X-ray crystallography S2

2. Materials and Methods for chemical synthesis S5
2.1 Synthesis of oligomer **2** S5
2.2 Experimental procedures S6

3. Solution studies S8
3.1 Circular dichroism titrations (Figures S1 to S3) S8
3.2 NMR studies (Figures S4 to S11) S9

4. NMR Structure assignment S14
4.1 (**2**)$_2$ ⊃ (D-**3**)$_2$ (Scheme S2; Figures S12 to S17; Tables S1 to S5) S14
4.2 (**2**)$_2$ ⊃ (D-**3**;D-**4**) (Scheme S3; Figures S18 to S21; Tables S6 to S8) S25

5. X-Ray Crystallography S33
5.1 X-Ray data for capsule **2.** (Tables S9; Figure S22) S33
5.2 X-Ray data for capsule (**2**)$_2$. (Tables S10; Figure S19) S35
5.3 X-Ray data for host-guest complex (**2**)$_2$ ⊃ (D-**3**)$_2$. (Tables S11; Figure S20-S21) S37

6. ^{1}H NMR and ^{13}C NMR spectra of new synthetic compounds S38

7. References S43

Other Supplementary Materials for this manuscript includes the following:

Crystallographic Information files for X-ray structures

1. Methods for NMR, Circular Dichroism and X-ray crystallography

Nuclear Magnetic Resonance. NMR spectra were recorded on 4 different NMR spectrometers: (1) an Avance II NMR spectrometer (Bruker Biospin) with a vertical 7.05T narrow-bore/ultrashield magnet operating at 300 MHz for ^{1}H observation and 75 MHz for ^{13}C observation by means of a 5-mm direct BBO H/X probe with Z gradient capabilities; (2) an Avance 400 NMR spectrometer (Bruker Biospin) with a vertical 9.4T narrow-bore/ultrashield magnet operating at 400 MHz for ^{1}H observation by means of a 5-mm direct QNP ^{1}H/^{13}C/^{31}P/^{19}F probe with gradient capabilities; (3) an Avance III NMR spectrometer (Bruker Biospin) with a vertical 16.45T narrow-bore/ultrashield magnet operating at 700 MHz for ^{1}H observation by means of a 5-mm TXI ^{1}H/^{13}C/^{15}N probe with Z gradient capabilities. (4) an Avance III NMR spectrometer (Bruker Biospin) with a Standard Bore Cryo Probe operating at 800 MHz for ^{1}H observation by means of a 5-mm TCI ^{1}H/^{13}C/^{15}N probe with Z gradient capabilities. Chemical shifts are reported in parts per million (ppm, δ) with tetramethylsilane as an internal standard. ^{1}H NMR splitting patterns with observed first-order coupling are designated as singlet (s), doublet (d), triplet (t), or quartet (q). Coupling constants (*J*) are reported in hertz. Data processing was performed with Topspin 3.5 software. Samples were not degassed. $CDCl_3$ from Sigma Aldrich was used after filtration through an alumina pad.

***NMR titrations*.** Titrations were performed in an NMR tube at 298.2 ± 0.1 K by adding aliquots of the stock solution of the guest by means of a Hamilton syringe to 0.500 mL solution of $(\mathbf{2})_2$. After homogenization and equilibration, NMR spectra were recorded.

***Solution state structure calculation*.** For structure determination of $(\mathbf{2})_2 \supset$ (D-**3**)$_2$ NMR spectra were initially collected at 298 K on a sample containing 2 mM $(\mathbf{2})_2$ and 4 mM ^{13}C-labelled D-**3** in CD_3Cl with 5 % (vol/vol) DMSO-d_6. Chemical shift assignment for all observable ^{1}H nuclei, as well as their colvalently attached ^{13}C and ^{15}N nuclei, were assigned based on 2D ^{1}H,^{13}C-HSQC, 2D ^{1}H,^{15}N-HSQC, 2D ^{13}C-HMBC, 2D ^{1}H-DQFCOSY, 2D x2-filtered ^{1}H-NOESY (150 ms mixing time), 3D ^{13}C-HSQC-NOESY (150 ms mixing time), 3D (H)CCH-TOCSY, and 3D H(C)CH-TOCSY spectra. These assignments are presented in Tables S1-S3. From the 2D NOESY, it was clear that significant chemical exchange was occurring, due to large crosspeaks observed for equivalent but spatially distant atoms in the two strands of the capsule double-helix. In order to calculate a high resolution structure it was necessary to repeat the NMR measurements at 278 K, which resulted in only minimal perturbation of the ^{1}H, ^{13}C and ^{15}N chemical shifts. Under these conditions, chemical exchange was almost completely suppressed on the timescale of the spectra acquition. Distance restraints were based on NOESY crosspeak intensities from two spectra. The 2D x2-filtered ^{1}H-NOESY (150 ms mixing time) was used to identify intramolecular $(\mathbf{2})_2$ nOe, and also intramolecular nOe between $(\mathbf{2})_2$ and D-**3**. This was due to selective filtering of protons bound to ^{13}C nuclei in the x2 dimension. The 3D ^{13}C-HSQC-NOESY (150 ms mixing time) was used to obtain intramolecular nOe within 13C-labelled D-**3**, as well as intermolecular nOe to $(\mathbf{2})_2$. The intensities from each spectra were calibrated based on the fixed distance of geminal aliphatic protons. The conformation of the bound D-**3** was validated by the pattern and intensity of crosspeaks in the 3D ^{13}C-HSQC-NOESY (150 ms mixing time), as well as crosspeak intensities in 2D ^{1}H-DQFCOSY and 2D ^{1}H-TOCSY acquired on a sample containing 1 mM $(\mathbf{2})_2$ and 2 mM natural abundance D-**3**. Calculation of 20 structures was performed with an MMFFs force field implemented within MacroModel (Maestro v6.5.007) and resulted in an ensemble of well-defined structures. Statistics of the final ensemble of 20 structures are included in Table S4.

For structure determination of (**2**)$_2$ ⊃ (D-**3**;D-**4**), significant perturbation and double the amount of new ^{1}H chemical shifts as compared to (**2**)$_2$ ⊃ (D-**3**)$_2$ necessitated a renewed chemical shift assignment process, once again at 298 K. Due to the increased complexity, four separate sample were prepared with different combinations of natural abundance and ^{13}C-labelled sugars, all in $CDCl_3$ with 5 % (v/v) DMSO-d_6: (*sample a*) 1 mM (**2**)$_2$, 1 mM ^{13}C-labelled D-**3**, 1 mM natural abundance D-**4**; (*sample b*) 1 mM (**2**)$_2$, 1 mM natural abundance D-**3**, 1 mM ^{13}C-labelled D-**4**, (*sample c*) 3 mM (**2**)$_2$, 3 mM ^{13}C-labelled D-**3**, 3 mM ^{13}C-labelled D-**4**; (*sample d*) 1 mM (**2**)$_2$, 1 mM natural abundance D-**3**, 1 mM natural abundance D-**4**. Assignment of the sugar resonances for the encapsulated D-**3,** D-**4** used a combination of ^{13}C-HSQC-NOESY (150 ms mixing time, on samples *a,b,c*), along with H(C)CH-TOCSY and (H)CCH-TOCSY (*sample c*). The assignment of the ^{1}H resconances of (**2**)$_2$ were obtained by first identifying chemical exchange pairs for the interior of the capsule, and next comparing each pair to the ^{1}H and ^{15}N resonances of the coexisting (**2**)$_2$ ⊃ (D-**3**)$_2$ by using ^{1}H,^{15}N-HSQC spectra. Validation and completion of the ^{1}H chemical shift assignment used intermolecular nOe crosspeaks of the resonances specific to (**2**)$_2$ ⊃ (D-**3,** D-**4**) by using 2D ^{1}H-NOESY (150 ms mixing time; *sample d*) and 2D x2-filtered ^{1}H-NOESY (150 ms mixing time; *samples b,c*). The resulting ^{1}H chemical shift assignments of (**2**)$_2$ ⊃ (D-**3,** D-**4**) are found in Table S5. Distance restraints were based on NOESY crosspeak intensities from three spectra. A 2D x2-filtered ^{1}H-NOESY (150 ms mixing time) was used to identify intramolecular (**2**)$_2$ nOe, and also intramolecular nOe between (**2**)$_2$ and D-**3** or D-**4**. 3D ^{13}C-HSQC-NOESY (150 ms mixing time) spectra were recorded two samples (*sample a, b*) to obtain intramolecular nOe within each ^{13}C-labelled sugar, as well as intermolecular nOe from each sugar to (**2**)$_2$, and also between D-**3** and D-**4**. The intensities from each spectra were calibrated based on the fixed distance of geminal aliphatic protons. Discrimination between nOe crosspeaks and exchange-derived crosspeaks was achieved by comparison to spectra recorded at 278 K, and by one round of iterative structure calculation. The conformation of the bound D-**3** and D-**4** was validated by the pattern and intensity of crosspeaks in the 3D ^{13}C-HSQC-NOESY (mixing time 150 ms; *samples b,c*), as well as crosspeak intensities in 2D ^{1}H-DQFCOSY and 2D ^{1}H-TOCSY (*sample d*). Calculation of 15 structures was performed with an MMFFs force field implemented within MacroModel (Maestro v6.5.007) and resulted in an ensemble of well-defined structures. Statistics of the final ensemble of 15 structures are included in Table S6.

Chemical exchange measurement. A series of ^{1}H,^{1}H-NOESY were collected for natural abundance (**2**)$_2$ ⊃ (D-**3**)$_2$ at 298 K and 278 K at a field strength of 700 MHz. At 298 K, the mixing times were 1, 5, 10, 25, 50, 100, 200, 400, 600, 800, 1000, 1200, 1400, 1600, 1800, and 2000 ms. Due to slower exchange at 278 K, only mixing times of 10,125, 250, 500, 750, 100, 1500 and 200 ms were used. The ratio of crosspeak intensity to diagonal peak intensity for two exchanging pairs were measured as a function of mixing time to produce an average of the values. The curves were fit with the equation (1-exp(-r*x))/(1+exp(-r*x) by using Qti plot (version 0.9.8). The fitted value of the exchange rate (r) represents the combined forward and reverse rate of exchange between the two conformations.

Circular Dichroism titrations. Titrations were performed in a 2 mm pathlength quartz cuvette at 298.2 ± 0.1 K by adding aliquots of the stock solution of the guests by means of a Hamilton syringe to 0.5 mL solution of (**2**)$_2$. After homogenization and equilibration CD spectra were recorded in the 340–390 nm region on a Jasco J-815 circular dichroism spectropolarimeter. Changes in ellipticity were analyzed using the HypSpec program.[1] The errors quoted are the standard deviations of the overall constants given directly by the program for the input data, which include all the wavelengths of each experimental point.

Crystallography. Data for compounds (**2**)$_2$ and and (**2**)$_2$ ⊃ (D-**3**)$_2$ were collected at the IECB X-ray facility (CNRS UMS 3033 – INSERM US001, University of Bordeaux). Single crystal X-ray diffraction experiments on (**2**)$_2$ were performed

on a High flux Bruker X8 Proteum rotating anode equipped with Helios optics and a Platinum CCD detector at the copper kα wavelength. The crystal was mounted on a cryo-loop after quick soaking on Paratone-N oil from Hampton research and flash-frozen. The diffractometer was composed of a kappa geometry goniometer allowing omega-scan data collections. The data were processed with the X8 proteum2suite.

Diffraction data for compound $(\mathbf{2})_2 \supset (\text{D-}\mathbf{3})_2$ were measured on a 3kW microfocus Rigaku FRX rotating anode. The source is equipped with high flux Osmic Varimax HF mirrors and a hybrid Dectris Pilatus 200K detector. The source is operating at the copper kα wavelength with a partial chi goniometer that decreases blind areas and enables automatic axial adjustment. Data were processed with the CrysAlisPro suite version 1.171.38.43.[2] Empirical absorption correction using spherical harmonics, implemented in SCALE3 ABSPACK scaling algorithm was used.

Both structures were solved with Shelxt and refined by full-matrix least-squares method on F2 with Shelxl-2014[3] within Olex2.[4] For all atoms, anisotropic atomic parameters were used. Hydrogen atoms were place at idealized position sand refined as riding of their carriers with Uiso(H)=1.2Ueq(CH, CH2, NH) and Uiso(H)=1.5Ueq(CH3). DFIX and AFIX instructions were used to improve the geometry of molecules and RIGU to model atomic displacement parameters. Severely disordered solvent molecules were removed using the SQUEEZE procedure from the PLATON suite.[5] For search and analysis of solvent accessible voids in the structures default parameters were utilized: grid 0.20 Å, probe radius 1.2 Å and NStep 6. Calculated total potential solvent accessible void volumes and electron counts per unit cell are given in the CIF files that were checked using IUCR's checkcif algorithm. Due to the characteristics of the crystals, i.e. large volume fractions of disordered solvent molecules, weak diffraction intensity, incompleteness of the data and moderate resolution, a number of A -level and B -level alerts remain in the check cif file. These alerts are inherent to the data and refinement procedures and do not reflect errors. In both structures A -level alerts related to the models accuracy concern the disordered "side chains" parts of the foldamers rather than the main chains.

Modelling. *Calculation of cavity volumes*. Cavity volumes of $(\mathbf{2})_2$ and of the $(\mathbf{2})_2 \supset (\text{D-}\mathbf{3})_2$ complex were estimated using the SURFNET software.[6] PDB-format files were generated from the x-ray data after removing encapsulated solvent and guest molecules and were used directly to calculate volumes. The volume of the cavities was generated by fitting spheres into the spaces generated between atoms (coordinate of the PDB files). Typically, the diameter of the probe used in this study was 1 Å. Packing coefficient is defined as the ratio between the volume of the guest and the volume of the cavity.

2. Materials and Methods for chemical synthesis

All reactions were carried out under a dry nitrogen atmosphere. Commercial reagents were purchased from Sigma-Aldrich, Alfa-Aesar or TCI and were used without further purification unless otherwise specified. Chloroform ($CHCl_3$) and diisopropylethylamine (DIEA) were distilled over calcium hydride (CaH_2) prior to use. Reactions were monitored by thin layer chromatography (TLC) on Merck silica gel 60-F254 plates and observed under UV light. GPC purification was performed on an LC-9130G NEXT setup (Japan Analytical Industry Co., Ltd.) equipped with two preparative columns (Inner diameter of 20mm and length of 600mm): a JAIGEL 2.5H and a JAIGEL 3H, in conjugation with UV-600 NEXT UV detector and an FC-3310 fraction collector. Chloroform with 1% EtOH and 0.5% Et_3N was used as mobile phase, with a flow rate of 7.0 mL/min. ESI mass spectra were obtained from the Mass Spectrometry Laboratory at the European Institute of Chemistry and Biology (UMS 3033 - IECB), Pessac, France.

2.1 Synthesis of oligomer 2

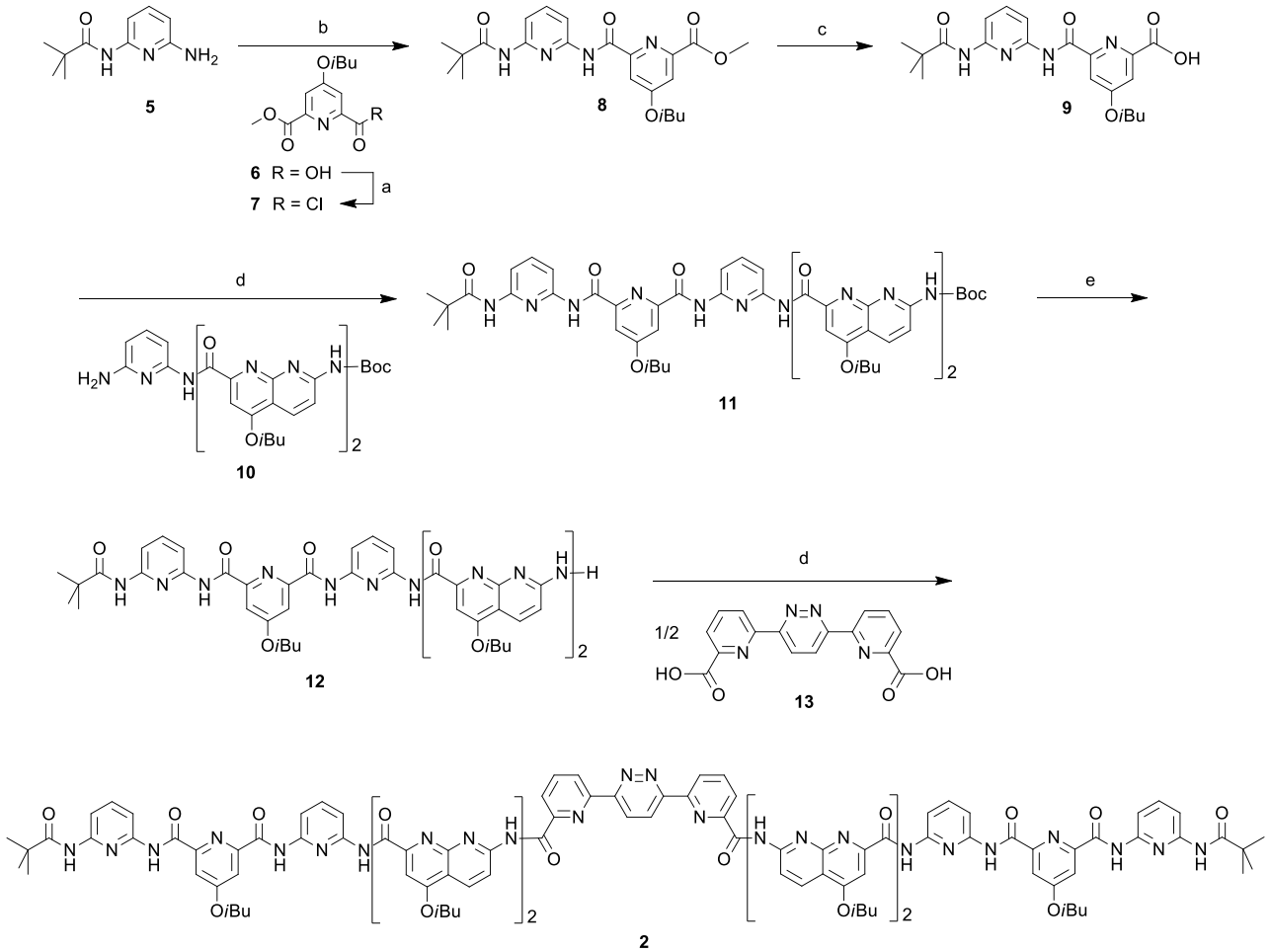

Scheme S1. Synthesis of oligomer **1**: (a) oxalyl chloride, dry $CHCl_3$, rt; (b) dry $CHCl_3$, DIPEA, rt; (c) NaOH 6M, 1,4-dioxane, 0ºC to rt; (d) dry $CHCl_3$, PyBOP, DIPEA, 40 °C; (e) TFA, $CHCl_3$, 0°C to rt, 2h.

2.2 Experimental procedures

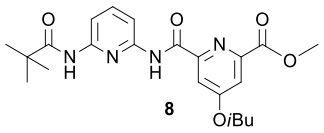

8

piv-P$_2$-ester (8). Monoester **6**[7] (0.449 g, 1.77 mmol) was dissolved in anhydrous $CHCl_3$ (2 mL). Oxalyl chloride (0.3 mL, 3.55 mmol) was added and the reaction was stirred at room temperature for 2.5 h. The solvents were removed under vacuum and the residue was dried under vacuum 6 h to yield acid chloride **7** as a yellow solid. The freshly prepared acid chloride **7** was dissolved in dry $CHCl_3$ (1 mL) and added dropwise at rt to a solution of **5**[8] (0.342 g, 1.77 mmol) and distilled DIPEA (1.8 mL, 10.33 mmol) in dry $CHCl_3$ (3mL). The reaction was allowed to proceed at rt for 12 h. The mixture was washed with sat. NH_4Cl, followed by sat. $NaHCO_3$ and finally water. The organic portions were dried with anydrous $MgSO_4$, filtered and evaporated to dryness. The residue was purified by precipitation from minimum amount of MeOH which gave **8** as a white solid (87%, 659 mg). ^{1}H NMR (300 MHz, $CDCl_3$) δ ppm = 10.29 (s, 1H); 8.08 (d, *J* = 8.00, 1H), 8.01 (d, *J* = 8.00, 1H), 7.94 (m, 1H), 7.91 (s, 1H), 7.79 – 7.74 (m, 2H), 4.04 (s, 3H), 3.93 (d, *J* = 6.40, 1H), 2.17, (m, 1H), 1.35 (s, 9H), 1.06 (d, *J* = 6.80, 6H). ^{13}C NMR (100 MHz, $CDCl_3$) δ ppm = 177.0, 167.8, 164.9, 161.7, 151.4, 150.1, 149.0, 148.2, 140.7, 115.1, 111.0, 109.7, 109.5, 75.3, 53.0, 39.8, 28.0, 27.5, 19.1. HRMS (ESI$^+$): *m/z* calcd for $C_{22}H_{29}N_4O_5$ $[M+H]^+$ 429.2138; found 429.2131.

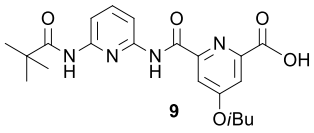

9

piv-P$_2$-acid (9). A solution of NaOH 6M (0.75 mL) was added to the ester **8** (657 mg, 1.53 mmol,) dissolved in 1,4-dioxane (7 mL) at 0ºC and the reaction mixture was stirred at rt overnight. The mixture was added to 5% aqueous citric acid solution (25 mL) and extracted with DCM. The organic portions were dried with anydrous $MgSO_4$, filtered and evaporated to dryness to give **9** as a white solid (93%, 591 mg). ^{1}H NMR (300 MHz, DMSO-d_6) δ ppm = 10.61 (s, 1H); 9.84 (s, 1H); 8.00 – 7.96 (m, 1H); 7.88 – 7.85 (m, 3H); 7.76 (d, *J* = 2.50, 1H); 4.05 (d, *J* = 6.50, 2H); 2.15 – 2.02 (m, 1H); 1.24 (s, 9H), 1.01 (d, *J* = 6.70, 6H. ^{13}C NMR (100 MHz, DMSO-d_6) δ ppm = 177.2, 167.5, 165.1, 161.3, 151.2, 150.5, 149.0, 148.9, 114.0, 111.3, 110.4, 108.8, 74.7, 27.5, 26.9, 18.8. HRMS (ESI$^+$): *m/z* calcd for $C_{21}H_{27}N_5O_5$ $[M+H]^+$ 415.1981; found 415.1978.

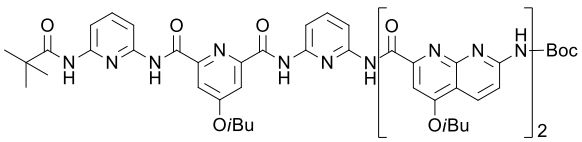

11

piv-P$_3$N$_2$-Boc (11). Acid **9** (322 mg, 0.73 mmol), amine **10**[9] (540 mg, 0.78 mmol) and PyBOP (2.058 mg, 4 mmol) were dissolved in dry $CHCl_3$ (10 mL). Then, DIPEA (0.683 mL, 0.119 mmol) and were added at room temperature and the reaction mixture was heated to 40 °C. After three days, the mixture was washed with sat. NH_4Cl, followed by sat. $NaHCO_3$ and finally water. The organic portions were dryed with anydrous $MgSO_4$, filtered and evaporated to dryness. The residue was purified by GPC to yield **11** as a white solid (58 %, 495 mg). ^{1}H NMR (300 MHz, $CDCl_3$) δ ppm = 11.01 (s, 1H); 10.58 (s, 1H); 9.99, (s, 2H); 8.71 (d, *J* = 8.95, 1H); 8.65 (d, *J* = 9.10, 1H); 8.51 (d, *J* = 9.20, 1H); 8.33 (d, *J* = 9.00, 1H);

8.21 (d, *J* = 8.00, 1H); 8.08 (t, *J* = 7.50, 2H); 7.97-7.95 (m, 3H), 7.84 (t, *J* = 7.90, 1H); 7.75-7.73 (m, 2H); 7.67 (s, 1H); 7.58 (t, *J* = 8.20, 1H); 4.14-4.10 (m, 4H); 3.96 (d, *J* = 6.50, 2H); 2.38-2.27 (m, 2H); 2.25-2.15 (m, 1H); 1.61 (s, 9H); 1.18 (d, *J* = 6.70, 6H); 1.16 (d, *J* = 6.70, 6H); 1.10 (d, *J* = 6.70, 6H); 0.94 (s, 9H). ^{13}C NMR (100 MHz, $CDCl_3$) δ ppm = 177.1, 168.2, 164.1, 163.9, 163.5, 162.4, 162.0, 161.5, 155.2, 154.7, 154.6, 154.2, 153.5, 152.4, 152.2, 150.8, 150.7, 150.1, 149.6, 149.4, 149.0, 140.5, 140.2, 134.3, 133.8, 115.1, 114.8, 114.2, 114.0, 112.3, 111.9, 110.8, 110.4, 110.3, 110.1, 98.9, 98.5, 82.0, 75.9, 75.8, 75.5, 39.5, 28.3, 28.2, 19.4, 19.2. HRMS (ESI$^+$): *m/z* calcd for $C_{57}H_{66}N_{13}O_{10}$ $[M+H]^+$ 1092.5056; found 1092.4697.

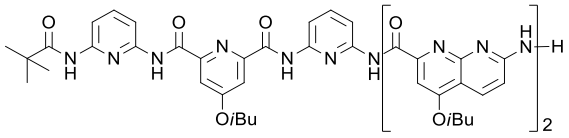

12

piv-P$_3$N$_2$-NH$_2$ (12). Trifluoroacetic acid (0.5 mL) was added dropwise to a solution of **11** (180 mg, 0.165 mmol) in 1.5 mL of $CHCl_3$ under nitrogen at 0 °C. Then, the resultant mixture was stirred at room temperature for 2 h. The volatiles were removed under reduced pressure to give a solid which was dissolved in DCM and washed two times with a saturated solution of $NaHCO_3$, distilled water and then with brine. The organic portions were dried with anydrous $MgSO_4$, filtered and evaporated to dryness to give **12** as a white solid (92%, 150 mg). ^{1}H NMR (300 MHz, DMSO-d_6) δ ppm = 11.75 (s, 1H); 11.45 (s, 1H); 11.08 (s, 1H), 10.82 (s, 1H), 9.38 (s, 1H), 8.76 (d, *J* = 8.80, 1H); 8.53 (d, *J* = 8.80, 1H); 8.16 (d, *J* = 8.80, 1H); 8.14-8.01 (m, 3H); 7.89-7.84 (m, 3H); 7.72 (s, 1H); 7.66 (t, *J* = 8.00, 1H); 7.50 (d, *J* = 8.00, 1H); 7.42 (s, 1H); 6.86 (d, *J* = 8.80, 1H); 6.78 (bs, 2H), 4.24 (d, *J* = 6.20, 2H); 4.09 (m, 4H); 2.29-2.05 (m, 3H); 1.11 (d, *J* = 6.70, 6H); 1.09 (d, *J* = 6.70, 6H); 1.05 (d, *J* = 6.70, 6H); 0.77 (s, 9H). Limited solubility of the product prevented characterization by ^{13}C NMR. HRMS (ESI$^+$): *m/z* calcd for $C_{52}H_{58}N_{13}O_8$ $[M+H]^+$ 992.4531; found 992.4501.

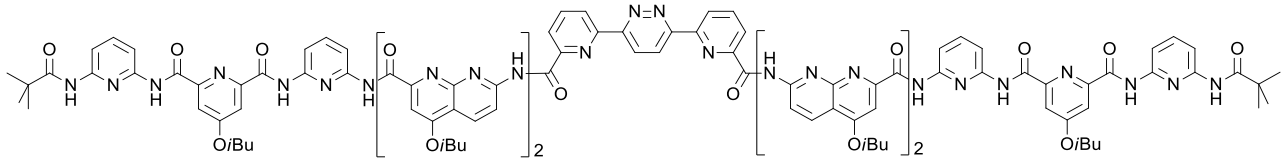

2

piv-P$_3$N$_2$pyrpyzpyrN$_2$P$_3$-piv (2). A solution of pentamer amine **12** (0.186 mmol, 185 mg), diacid **13**[9] (0.093 mmol, 30 mg) and PyBOP (0.93 mmol, 484 mg) were dissolved in dry $CHCl_3$ (2 mL). Then, DIPEA (0.93 mmol, 0.162 mL) was added at rt and the reaction mixture was heated to 40ºC for 2 days. The solvents were removed under reduced pressure and the residue was purified by GPC which gave **2** as a white solid (84%, 177 mg). ^{1}H NMR (300 MHz, $CDCl_3$) δ ppm = 9.90 (s, 2H); 9.87 (s, 2H); 9.55, (s, 2H), 9.30, (s, 2H), 8.81, (s, 2H), 8.68 (s, 2H), 8.58, (s, 2H), 8.24 (d, *J* = 8.80, 2H); 8.10 (d, *J* = 8.80, 2H); 8.00 (m, 2H); 7.78 (m, 2H); 7.57 (m, 2H); 7.44-7.30 (m, 6H), 7.17 (t, *J* = 8.00, 3H); 7.11 (s, 3H); 7.02 (t, *J* = 7.80, 2H); 6.91-6.88 (m, 4H); 6.82 (d, *J* = 7.80, 2H); 6.53 (s, 2H); 6.44 (t, *J* = 8.00, 2H); 4.03-3.89 (m, 6H); 3.83-3.66 (m, 6H); 2.45-2.33 (m, 2H); 2.32-2.21 (m, 2H); 2.16-2.05 (m, 2H); 1.31 (d, *J* = 6.70, 6H); 1.30 (d, *J* = 6.70, 6H); 1.23 (d, *J* = 7.80, 6H); 1.20 (d, *J* = 7.80, 6H); 1.11 (d, *J* = 6.70, 6H); 1.10 (d, *J* = 6.70, 6H); 0.36 (s, 18H). ^{13}C NMR (100 MHz, $CDCl_3$) δ ppm = 177.5, 167.3, 163.0, 162.9, 161.7, 160.7, 160.6, 160.4, 156.0, 153.2, 153.1, 152.6, 152.5, 152.1, 151.8, 151.1, 150.5, 149.7, 149.2, 148.7, 148.5, 148.2, 146.9, 139.5, 138.9, 137.4, 134.5, 132.3, 129.9, 126.1, 125.4, 122.2, 115.0, 113.8, 113.1, 112.9, 112.3, 111.0, 110.6, 110.1, 108.1, 98.2, 97.4, 75.8, 75.4, 75.1, 39.0, 29.9, 28.4, 28.3, 28.1, 26.8, 19.6, 19.5, 19.2. HRMS (ESI$^+$): *m/z* calcd for $C_{120}H_{121}N_{30}O_{18}$ $[M+H]^+$ 2270.9509; found 2270.9513.

3. Solution studies

3.1 Circular dichroism titrations (enlarged versions of the main text Figures)

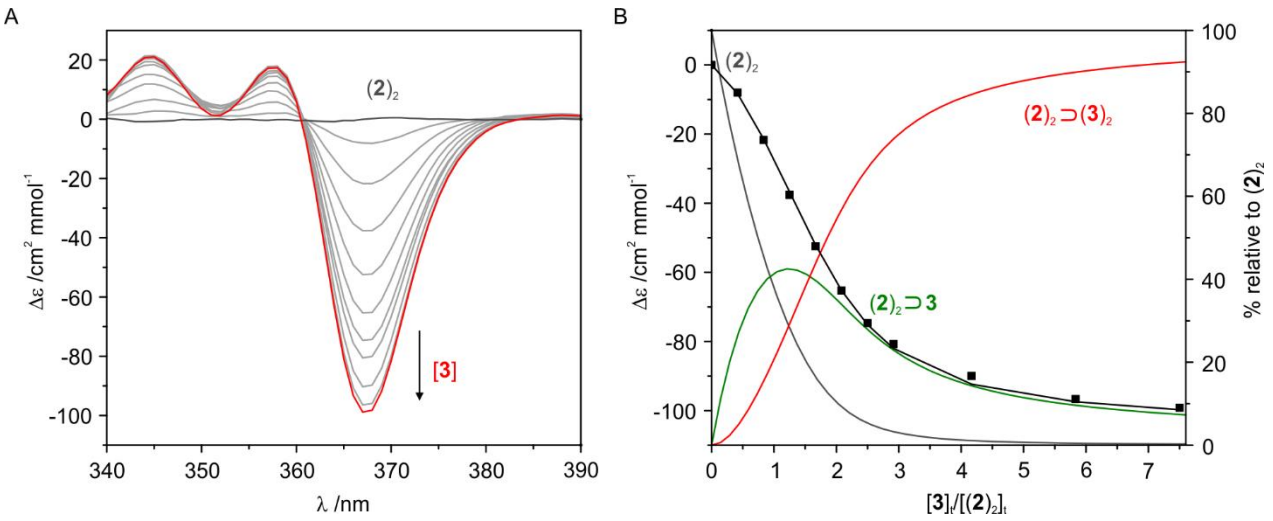

Figure S1. (A) Induced CD spectra upon binding of D-**3** by (**2**)$_2$ in $CHCl_3$/DMSO (9:1 vol/vol) at 298K, [(**2**)$_2$] = 96 μM. The red colored line corresponds to 7.5 equiv. of D-**3** added; (B) Experimental (■) and calculated values (–) for the ICD binding study of receptor (**2**)$_2$ vs. D-**3** with the corresponding species distribution diagram. Although only Δε values at 367 nm are shown here, all wavelengths in the 340–390 nm region were used for the calculation of the binding constants. K_{a1} = 69180 M^{-1}; K_{a2} = 31620 M^{-1}. Limiting Δε = –105 cm^2 $mmol^{-1}$;

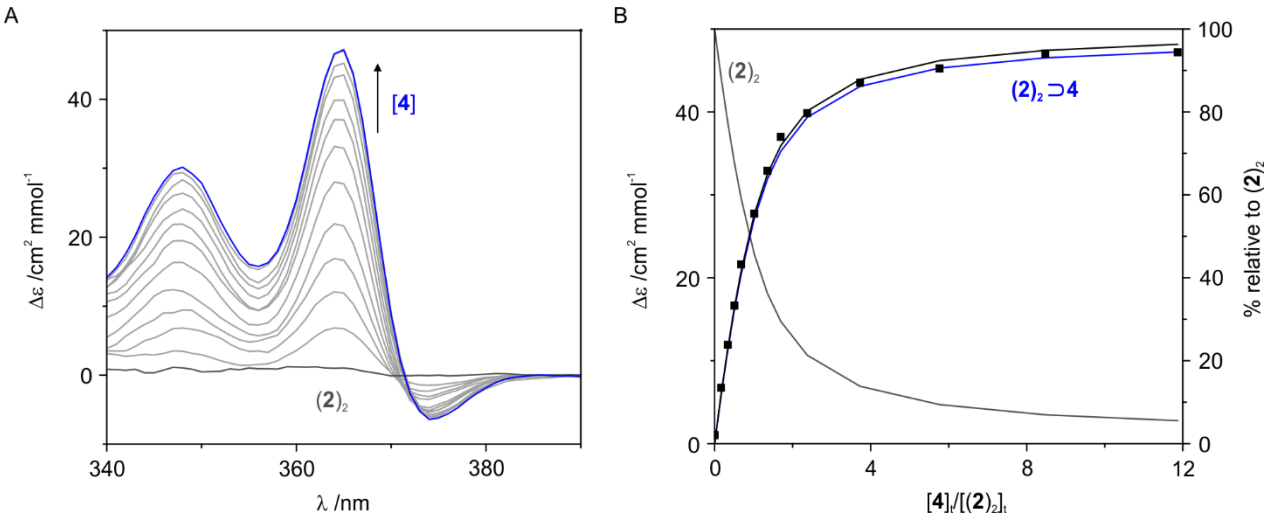

Figure S2. (A) Induced CD spectra upon binding of D-**4** by (**2**)$_2$ in $CHCl_3$/DMSO (9:1 vol/vol) at 298 K, [(**2**)$_2$] = 120 μM. The blue colored line corresponds to 12 equiv. of D-**4** added. (B) Experimental (■) and calculated values (–) for the ICD binding study of receptor (**2**)$_2$ vs. D-**4** with the corresponding species distribution diagram. Although only Δε values at 365 nm are shown here, all wavelengths in the 340–390 nm region were used for the calculation of the binding constant. K_a = 21900 M^{-1}. Limiting Δε = 51 cm^2 $mmol^{-1}$.

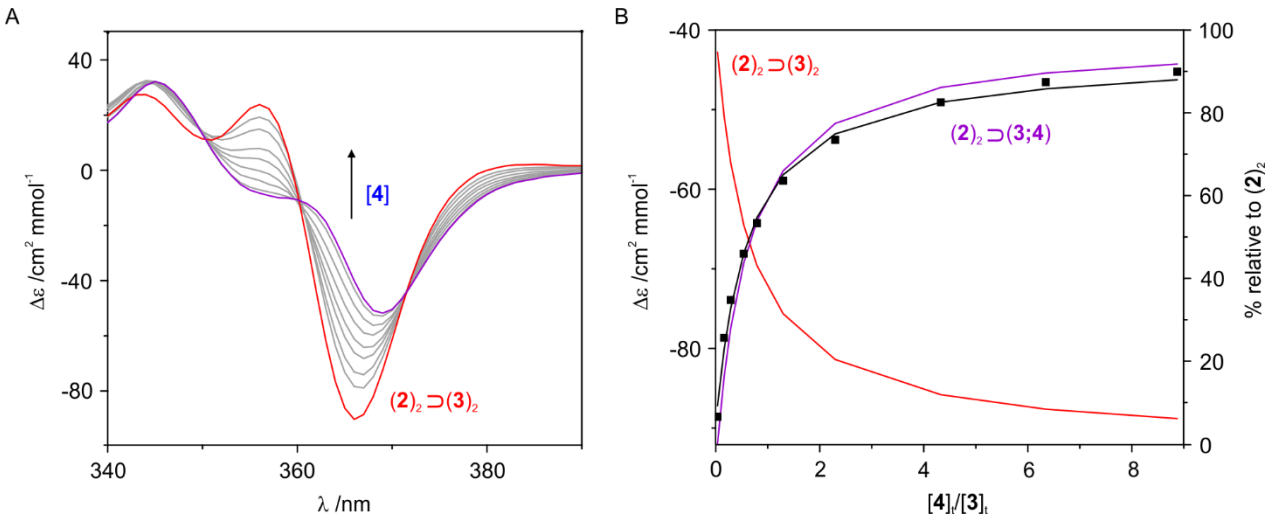

Figure S3. (A) Changes in the CD spectra of (**2**)$_2$⊃(D-**3**)$_2$ upon binding of D-**4** in $CHCl_3$/DMSO (9:1 vol/vol) at 298 K. [(**2**)$_2$] = 94 μM; [D-**3**] = 755 μM. The purple colored line corresponds to 8.5 equiv. of D-**4** added, relative to D-**3**; (B) Experimental (■) and calculated values (–) for the ICD binding study of (**2**)$_2$⊃(D-**3**)$_2$ vs. D-**4** with the corresponding species distribution diagram. Although only Δε values at 367 nm are shown here, all wavelengths in the 340–390 nm region were used for the calculation of the binding constant. K_a = 46800 M^{-1} for the equilibrium (**2**)$_2$⊃D-**3** + D-**4** ⇌ (**2**)$_2$⊃(D-**3**,D-**4**). Limiting Δε = –45 cm^2 $mmol^{-1}$.

3.2 NMR studies

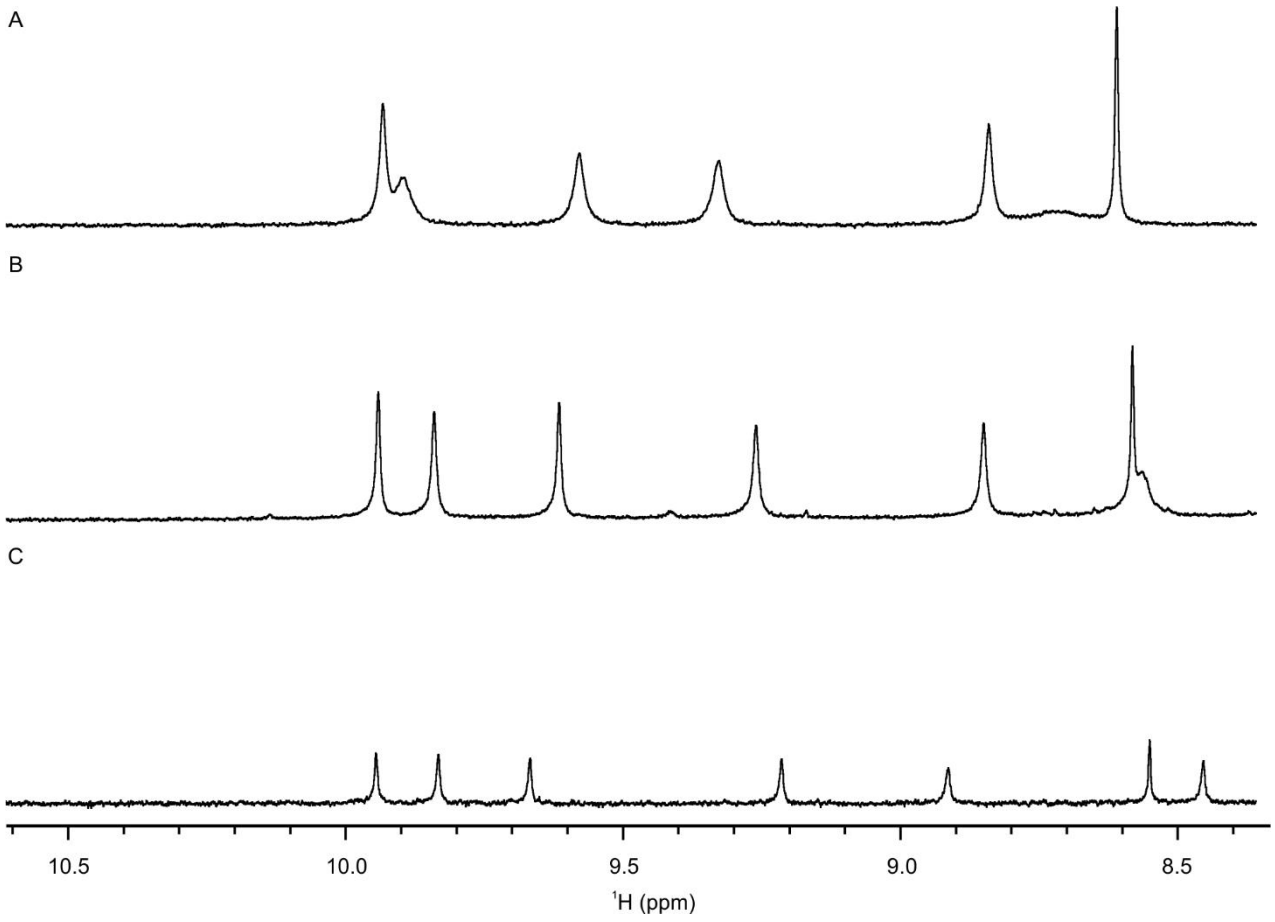

Figure S4. Excerpts from the 400 MHz ^{1}H NMR spectra showing the amide resonance region of (**2**)$_2$ in $CDCl_3$ at 1 mM (A); 0.25 mM (B) and 0.05 mM (C) in $CDCl_3$ at 298K.

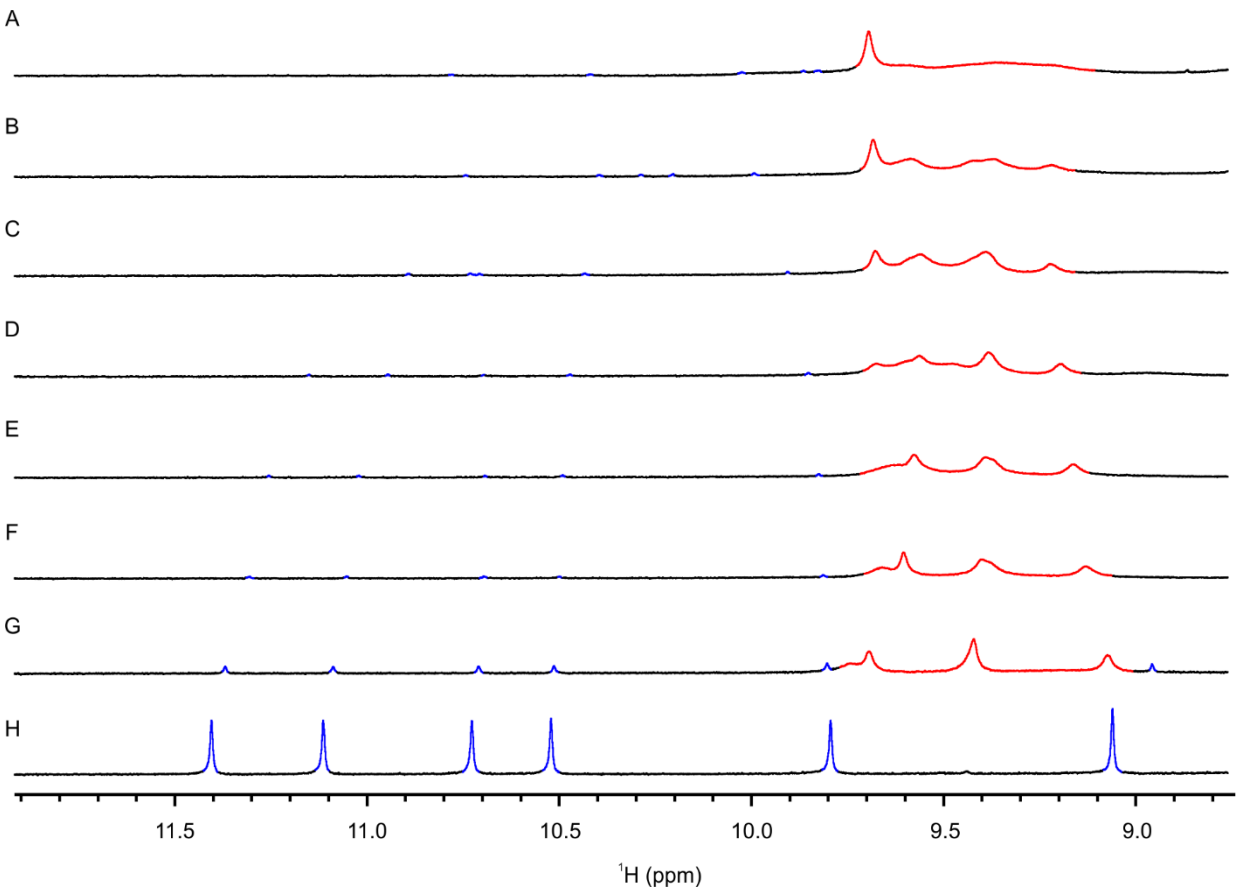

Figure S5. Excerpts of the 400 MHz ^{1}H NMR spectra at 298 K showing the amide resonance region of **2** at 1 mM in various $CDCl_3$/DMSO-d_6 proportions (vol/vol): 9.5:0.5 (A); 9:1 (B); 8:2 (C); 7:3 (D); 6:4 (E); 5:5 (F); 7.5:2.5 (G) and neat DMSO-d_6 (H). Resonances highlighted in red belong to the double helical form, $(\mathbf{2})_2$, while those depicted in blue correspond to the single helix **2**. The spectum at 9:1 vol/vol was used to determine K_{dim} which was found to be 400000 M^{-1} in this solvent system.

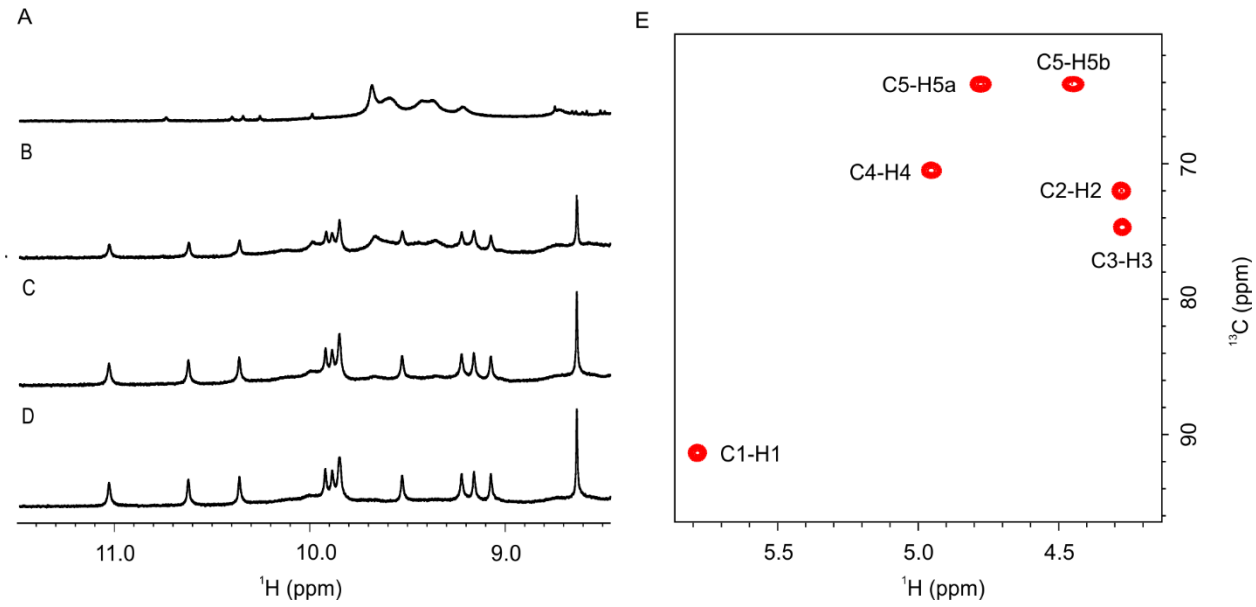

Figure S6. Excerpts from the 400 MHz ^{1}H NMR spectra showing the amide resonances of $(\mathbf{2})_2$ at 1 mM (298K) in $CDCl_3$/DMSO-d_6 (9:1 vol/vol) in the presence of (A) 0 equiv.; (B) 1 equiv.; (C) 2 equiv. and (D) 3 equiv. of D-**3**. (E) Excerpt of the ^{1}H,^{13}C HSQC spectrum showing correlation signature of two encapsulated uniformly ^{13}C-labelled α-$^4C_1$-D-xylopyranose **3** ($CDCl_3$/DMSO-d_6 9:1 vol/vol).

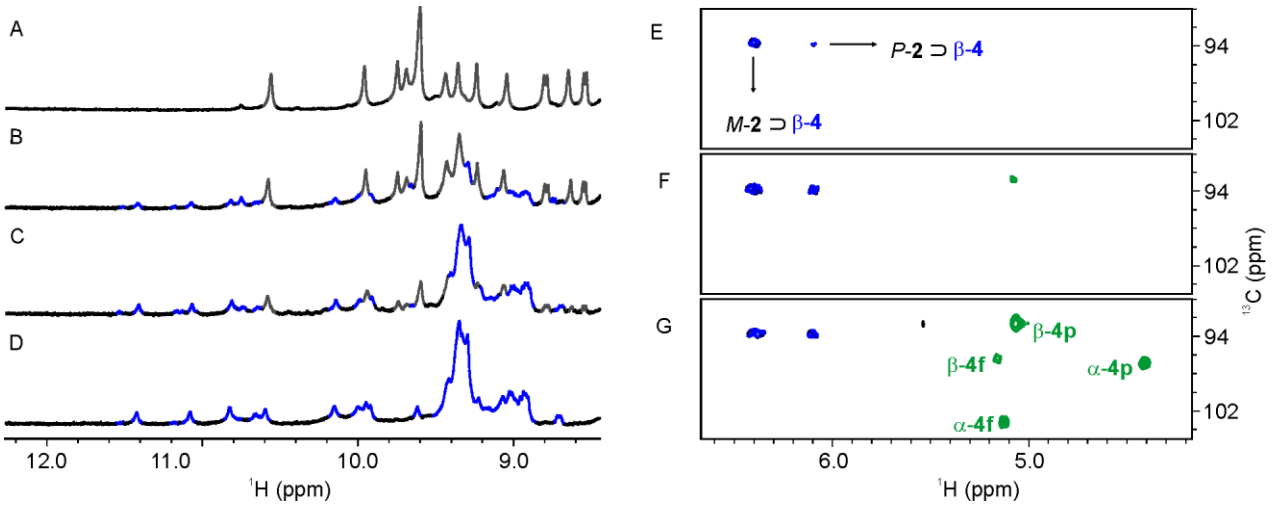

Figure S7. Excerpts from the 400 MHz ^{1}H NMR spectra showing the amide resonances of capsule (**2**)$_2$ at 1 mM in $CDCl_3$/DMSO-d_6 (9:1 vol/vol) and 243K in the presence of (A) 0 equiv.; (B) 0.5 equiv.; (C) 1.0 equiv. and (D) 2.0 equiv. of D-**4**. Excerpts from ^{1}H-^{13}C HSQC spectra showing the ^{1}H correlations of C1 (anomeric carbon) of uniformly ^{13}C-labelled β-$^1C_4$-D-arabinopyranose recorded in the following conditions: (E) [(**2**)$_2$] = 1.0 mM; [D-**4**]= 0.5 mM; (F) [(**2**)$_2$] = 1.0 mM; [D-**4**]= 1.0 mM; (G) [(**2**)$_2$] = 1.0 mM; [D-**4**]= 2.0 mM. Encapsulated and free forms of the sugar are represented in blue and green, respectively. All solutions were prepared in $CDCl_3$/DMSO-d_6 (9:1 vol/vol) and the spectra recorded at 298K.

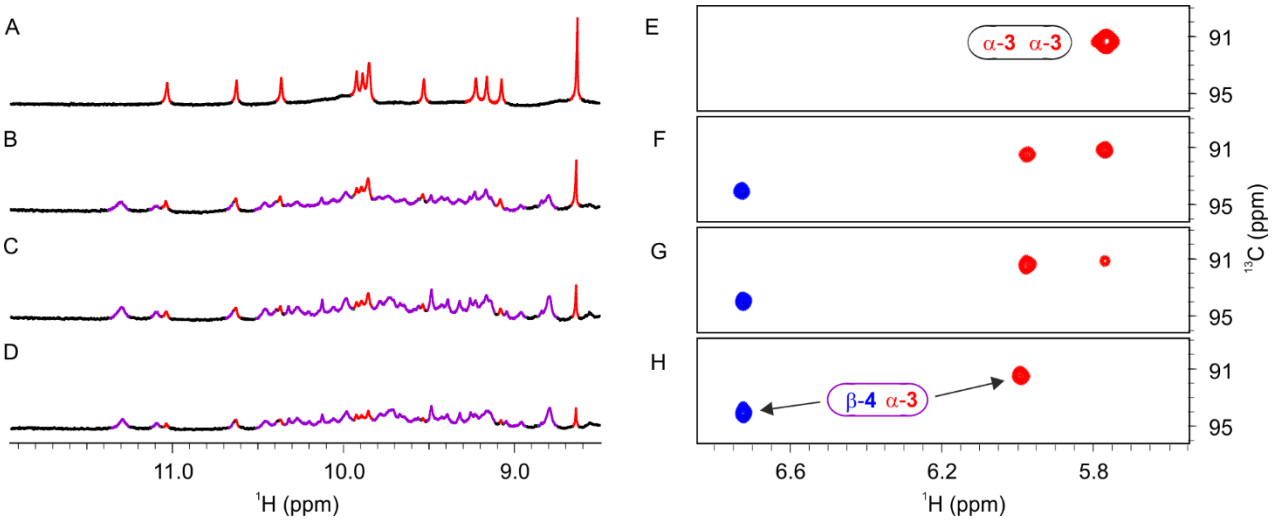

Figure S8. Excerpts from the 400 MHz ^{1}H NMR spectra showing the amide resonances of (**2**)$_2$⊃(D-**3**)$_2$ at 1 mM in $CDCl_3$/DMSO-d_6 (9:1 vol/vol) and 298K in the presence of (A) 0 equiv.; (B) 1 equiv.; (C) 2 equiv. and (D) 3 equiv. of D-**4** relative to D-**3**. (**2**)$_2$⊃(D-**3**)$_2$ and (**2**)$_2$⊃(D-**3**,D-**4**) amide resonances are shown in red and purple, respectively. Excerpts from ^{1}H-^{13}C HSQC spectra recorded in $CDCl_3$/DMSO-d_6 (9:1 vol/vol) and 298K showing the ^{1}H correlations of C1 of encapsulated uniformly ^{13}C-labelled α-$^4C_1$-D-xylopyranose and β-$^1C_4$-D-arabinopyranose recorded in the following conditions: (E) [(**2**)$_2$] = 1.0 mM; [**3**] = 2.0 mM; previous solution plus (F) [**4**]= 2.0 mM; (G) [**4**] = 6.0 mM. (H) at 318K. C1 correlations of D-**3** and D-**4** are represented in red and blue, respectively.

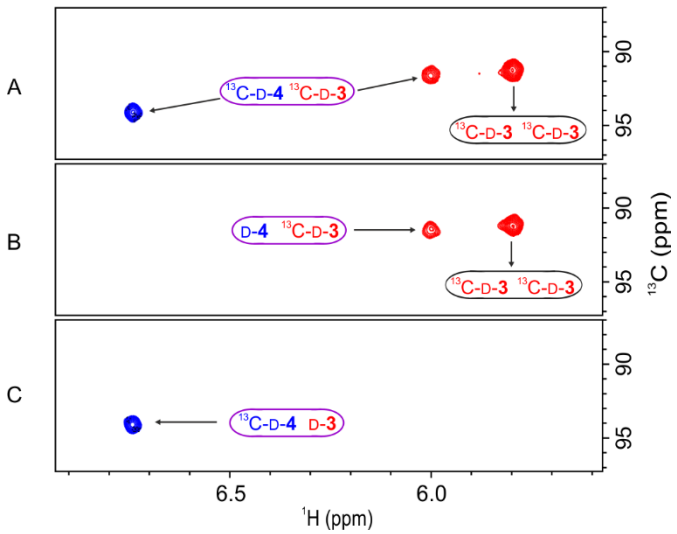

Figure S9. Excerpts from ^{1}H-^{13}C HSQC spectra of solutions with [(**2**)$_2$] = [**3**] = [**4**] = 1.0 mM prepared in $CDCl_3$/DMSO-d_6 (9:1 vol/vol) and 298K, showing the ^{1}H correlations of C1 of encapsulated uniformly ^{13}C-labelled sugars: (A) both sugars labelled; (B) labelled D-**3** and unlabeled D-**4**; (C) unlabelled D-**3** and labeled D-**4**.

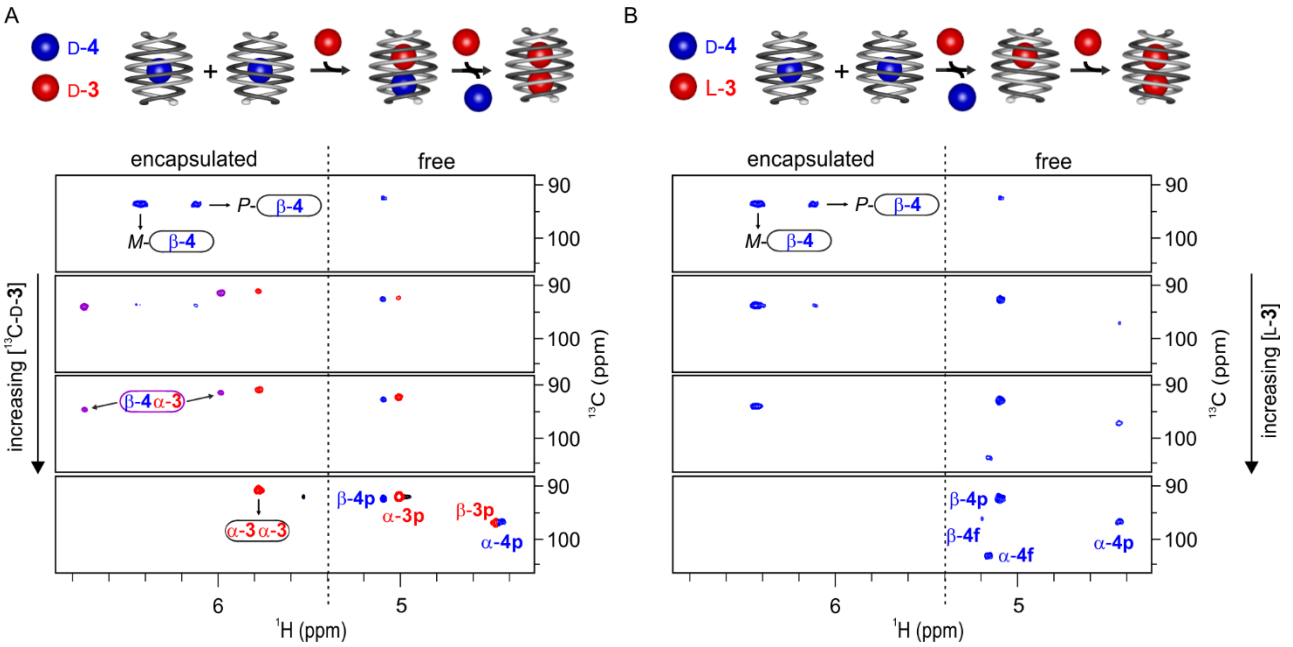

Figure S10. (A) Titration performed in $CDCl_3$/DMSO-d_6 (9:1 vol/vol) and 298K using both uniformly ^{13}C-labelled D-**3** and D-**4**, monitored by ^{1}H-^{13}C HSQC. The starting spectra shows two ^{1}H-^{13}C correlations for the anomeric C1 carbon of D-**4** encapsulated in (**2**)$_2$ which is attributed to a unique tautomer of D-**4** being encapsulated either in a *P* or *M* helices of (**2**)$_2$. Upon increasing the concentration of D-**3** three new correlations appear: two correspond to (**2**)$_2$ ⊃ (D-**3**;D-**4**) (in purple) and the other to the (**2**)$_2$ ⊃ (D-**3**)$_2$ complex. Adding excess D-**3** eventually leads to complete replacement of D-**4** by D-**3** and to exclusive formation of (**2**)$_2$ ⊃ (D-**3**)$_2$. (B) Titration performed in $CDCl_3$/DMSO-d_6 (9:1 vol/vol) and 298K using uniformly ^{13}C-labelled D-**4** and non-labelled L-**3** (the ^{13}C-labelled L-enantiomer is not commercially available), monitored by ^{1}H-^{13}C HSQC. The starting spectrum shows again the two ^{1}H-^{13}C correlations for the anomeric C1 carbon of D-**4** encapsulated in *P* and *M* helices of (**2**)$_2$. Upon increasing the concentration of L-**3** only correlations corresponding to free D-**4** appear, indicating no heterocomplex forms and only the (**2**)$_2$ ⊃ (L-**3**)$_2$ complex predominates (not visible since L-**3** is unlabeled). In both (A) and (B), the host is 1mM, starting spectrum has 1 equiv of D-**4** and the others have 0.5, 1 and 4 equiv (top to bottom) of either D-**3** or L-**3**. Only the spectral region of the ^{1}H correlations of C1 of the sugars are shown.

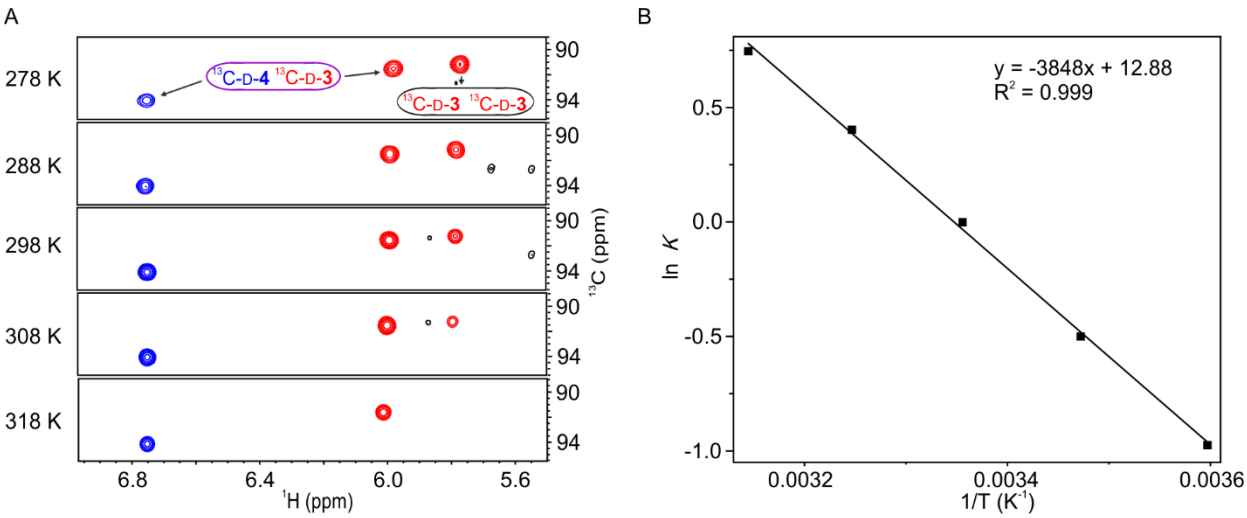

Figure S11. Excerpts from ^{1}H-^{13}C HSQC spectra of solutions with [(**2**)$_2$] = 0.1 mM; [**3**] = 0.2 mM; [**4**] = 0.4 mM prepared in $CDCl_3$/DMSO-d_6 (9:1 vol/vol) and 298K, showing the ^{1}H correlations of C1 of encapsulated uniformly ^{13}C-labelled sugars at the indicated temperatures (A) and corresponding Van't Hoff plot. $\Delta\Delta H$=32 kJ mol^{-1}; $\Delta\Delta S$=0.11 kJ mol^{-1} K^{-1}.

4. NMR structure assignments

4.1 NMR structure of the $(2)_2 \supset (D\text{-}3)_2$

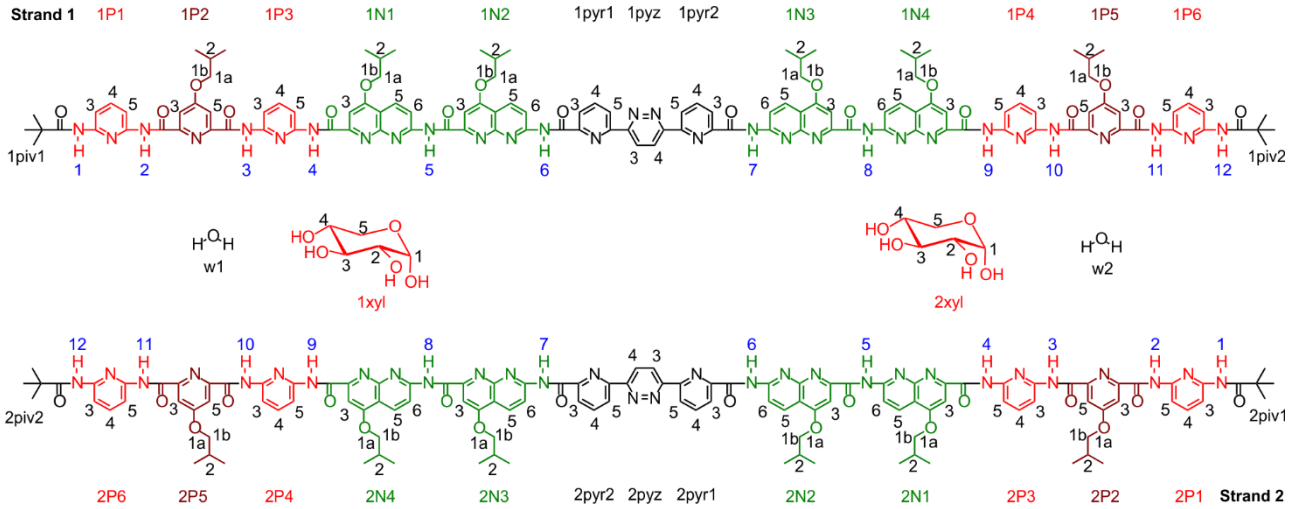

Scheme S2. Labelling of the $(\mathbf{2})_2 \supset (D\text{-}\mathbf{3})_2$.

Table S1. Full assignment of the ^{1}H chemical shifts of $(\mathbf{2})_2 \supset (D\text{-}\mathbf{3})_2$ in $CDCl_3$/DMSO-d_6 (95:5) at 298K (800 MHz).

Monomer	Atom	^{1}H (ppm)	Monomer	Atom	^{1}H (ppm)
1piv1	CH_3	0.072	2piv1	CH_3	0.072
1P1	NH1	7.334	2P1	NH1	7.334
	H3	6.489		H3	6.489
	H4	6.610		H4	6.610
	H5	6.453		H5	6.453
	NH2	10.358		NH2	10.358
1P2	H3	7.467	2P2	H3	7.467
	H5	7.153		H5	7.153
	H1a	3.813		H1a	3.813
	H1b	3.735		H1b	3.735
	H2	2.068		H2	2.068
1P3	NH3	9.832	2P3	NH3	9.832
	H3	7.200		H3	7.200
	H4	7.223		H4	7.223
	H5	7.650		H5	7.650
	NH4	9.908		NH4	9.908
1N1	H3	6.538	2N1	H3	6.538
	H5	8.096		H5	8.096
	H6	8.071		H6	8.071
	H1a	3.464		H1a	3.464
	H1b	3.690		H1b	3.690
	H2	2.132		H2	2.132
	NH5	10.576		NH5	10.576
	H3	7.137		H3	7.137

1N2	H5	8.281	2N2	H5	8.281
	H6	8.113		H6	8.113
	H1a	3.963		H1a	3.963
	H1b	3.884		H1b	3.884
	H2	2.326		H2	2.326
	NH6	9.493		NH6	9.493
1pyr1	H3	8.014	2pyr1	H3	8.014
	H4	7.992		H4	7.992
	H5	8.401		H5	8.401
1pyz	H3	8.589	2pyz	H3	8.589
	H4	8.581		H4	8.581
1pyr2	H4	7.220	2pyr2	H4	7.220
1N3	NH7	9.163	2N3	NH7	9.163
	H6	7.968		H6	7.968
	H5	7.585		H5	7.585
	H3	6.846		H3	6.846
	H1a	3.714		H1a	3.714
	H1b	3.967		H1b	3.967
	H2	2.139		H2	2.139
1N4	NH8	10.998	2N4	NH8	10.998
	H6	7.696		H6	7.696
	H5	7.895		H5	7.895
	H3	6.561		H3	6.561
	H1a	3.660		H1a	3.660
	H1b	3.909		H1b	3.909
	H2	2.320		H2	2.320
1P4	NH10	9.845	2P4	NH10	9.845
	H5	7.454		H5	7.454
	H4	6.807		H4	6.807
	H3	7.310		H3	7.310
	NH9	9.128		NH9	9.128
1P5	H5	6.540	2P5	H5	6.540
	H3	6.404		H3	6.404
	H1a	3.203		H1a	3.203
	H1b	3.310		H1b	3.310
	H2	1.881		H2	1.881
1P6	NH11	9.070	2P6	NH11	9.070
	H5	6.242		H5	6.242
	H4	5.493		H4	5.493
	H3	6.378		H3	6.378
	NH12	9.877		NH12	9.877
1piv2	CH_3	0.880	2piv2	CH_3	0.880
1xyl	H1	5.727	2xyl	H1	5.727
	H2	4.234		H2	4.234
	H3	4.216		H3	4.216
	H4	4.885		H4	4.885
	H5a	4.386		H5a	4.386
	H5b	4.710		H5b	4.710

	OH1	7.447		OH1	7.447
	OH2	5.299		OH2	5.299
	OH3	8.150		OH3	8.150
	OH4	5.292		OH4	5.292

Table S2. ^{13}C chemical shift assignment of $(\mathbf{2})_2 \supset (D\text{-}\mathbf{3})_2$ in $CDCl_3$/DMSO-d_6 (95:5) at 298K (800 MHz).

Monomer	Atom	^{13}C (ppm)	Monomer	Atom	^{13}C (ppm)
1piv1	CH_3	25.554	2piv1	CH_3	25.554
1P1	CO	176.004	2P1	CO	176.004
	C3	109.874		C3	109.874
	C4	137.672		C4	137.672
	C5	111.205		C5	111.205
1P2	CO	166.531	2P2	CO	166.531
	C1	74.558		C1	74.558
	C2	27.496		C2	27.496
	C3	110.397		C3	110.397
	C5	112.493		C5	112.493
	CO	160.718		CO	160.718
1P3	C4	135.744	2P3	C4	135.744
	C5	110.706		C5	110.706
1N1	CO	161.308	2N1	CO	161.308
	C1	74.123		C1	74.123
	C3	96.625		C3	96.625
	C5	132.216		C5	132.216
	C6	114.958		C6	114.958
1N2	C1	75.388	2N2	C1	75.388
	C2	27.673		C2	27.673
	C3	98.301		C3	98.301
	C5	134.426		C5	134.426
	C6	113.285		C6	113.285
1pyr1	C3	123.318	2pyr1	C3	123.318
	C4	138.077		C4	138.077
	C5	125.347		C5	125.347
1pyz	C3	122.041	2pyz	C3	122.041
	C4	124.558		C4	124.558
1N3	C1	75.186	2N3	C1	75.186
	C2	27.689		C2	27.689
	C3	97.953		C3	97.953
	C5	131.544		C5	131.544
	C6	114.694		C6	114.694
1N4	CO	159.433	2N4	CO	159.433
	C1	75.008		C1	75.008
	C2	27.723		C2	27.723
	C3	97.421		C3	97.421
	C5	133.766		C5	133.766

	C6	114.444		C6	114.444
1P4	C3	108.243	2P4	C3	108.243
	C4	139.647		C4	139.647
	C5	108.208		C5	108.208
1P5	CO	160.306	2P5	CO	160.306
	C1	74.096		C1	74.096
	C2	27.255		C2	27.255
	C3	109.498		C3	109.498
	C4	165.114		C4	165.114
	C5	108.310		C5	108.310
	CO	160.139		CO	160.139
1P6	C3	109.162	2P6	C3	109.162
	C4	136.454		C4	136.454
	C5	110.735		C5	110.735
	CO	176.808		CO	176.808
1piv2	$\underline{C}H_3$	26.093	2piv2	$\underline{C}H_3$	26.093

Table S3. Full assignment of the hydrogen-bound ^{15}N chemical shifts of $(\mathbf{2})_2 \supset (\text{D-}\mathbf{3})_2$ in $CDCl_3$/DMSO-d_6 (95:5) at 298K (800 MHz).

Monomer	Atom	^{15}N (ppm)	Monomer	Atom	^{15}N (ppm)
1P1	N1	132.566	2P1	N1	132.566
1P1	N2	130.605	2P1	N2	130.605
1P3	N3	130.930	2P3	N3	130.930
1P3	N4	129.685	2P3	N4	129.685
1N1	N5	133.198	2N1	N5	133.198
1N2	N6	128.134	2N2	N6	128.134
1N3	N7	131.556	2N3	N7	131.556
1N4	N8	136.183	2N4	N8	136.183
1P4	N10	131.896	2P4	N10	131.896
1P4	N9	127.384	2P4	N9	127.384
1P6	N11	130.868	2P6	N11	130.868
1P6	N12	134.732	2P6	N12	134.732

Table S4. NMR statistics for the ensemble of twenty structures of $(\mathbf{2})_2 \supset (\text{D-}\mathbf{3})_2$.

NMR distance restraints	
Total	334
Capsule-capsule	190
Sugar-capsule	82
Sugar-sugar	48
Water-sugar	12
Water-capsule	2
Structure statistics (mean and standard deviation)	
Violations	
Distance restraints (Å)	0.012±0.002
Energy (kJ/mol)	460±10
Minimization Energies (kJ/mol)[a]	
Total	-121±20
Stretch	269.8±0.7
Bend	1328±12
Tortion	200±2
Improper torsion	8.8±0.4
VDW	2866±3
Electrostatic	-4948±2
Cross terms	-22±2
Solvation	-293±2
rmsd between 6220 atoms pairs (Å)	
1.025	

[a] Final energies from minimization by using MMFFs (Maestro v. 6.5.007)

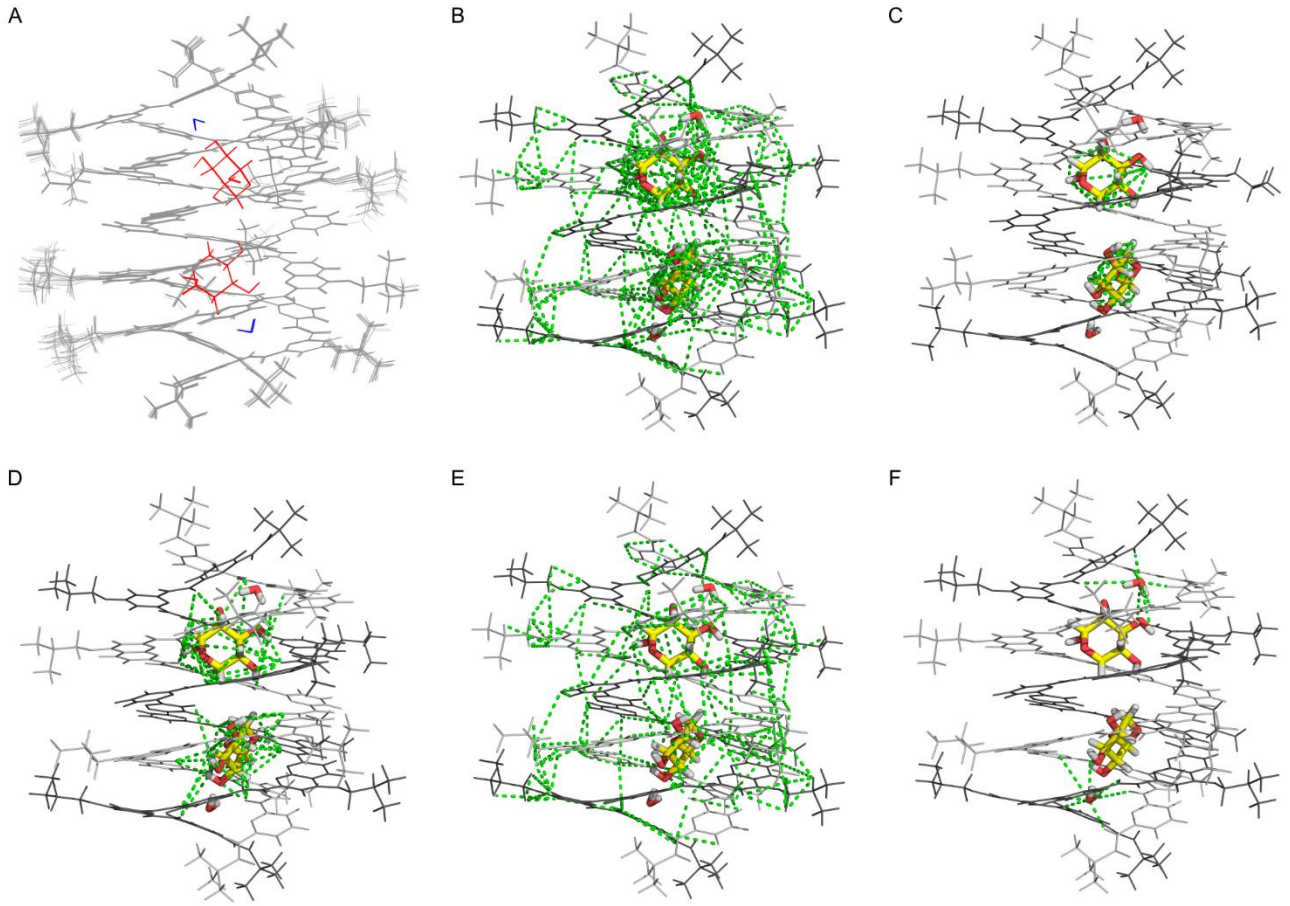

Figure S12. High-resolution NMR structure of the $(\mathbf{2})_2 \supset (\text{D-}\mathbf{3})_2$ complex. (A) ensemble of 20 structures. (B) Distance restraints used to calculate the ensemble of 20 structures. Dotted green lines indicate the complete set of 336 distance restraints mapped onto a representative structure from the ensemble. (C) Location of the 48 intramolecular xylose restraints that confirm the α-$^4C_1$-pyranose conformation of the encapsulated guests. (D) Location of the 82 intermolecular capsule-xylose restraints used to position the guests within the capsule. (E) Location of the 190 inter- and intra-strand restraints to position the strands relative to one another, as well as the side chains. (F) Location of the 14 distance restraints used to position the water molecules. In all representations each strand is shown in tube representation and colored in a different tone of gray. Oxygen atoms are colored in red; carbon atoms of the guests are colored in yellow.

Table S5. OH···N, NH···O and OH···O hydrogen bonding distances in the (**2**)$_2$ ⊃ (D-**3**)$_2$ complex as found in the NMR structure.[a]

	***d* (Å)**[b]
(1P1)NH1···O(w1)	2.707(4)
(1P2)NH3···O(w1)	2.16(2)
(2P6)NH12···O(w1)	2.178(8)
(w1)OH1···O3(xyl1)	1.95(2)
(w1)OH1···N(1P3)	2.18(2)
(w1)OH2···O4(xyl1)	2.63(4)
(xyl1)OH2···N(2P4)	2.30(3)
(2P6)NH11···O3(xyl1)	2.31(4)
(1P3)NH4···O4(xyl1)	2.47(3)
(xyl1)OH3···N(2N4)	1.881(3)
(2N4)NH8···O5(xyl1)	1.741(1)
(xyl1)OH4···N(2N3)	2.046(2)
(1N1)NH5···O1(xyl1)	2.079(9)
(xyl1)OH1···N(1N2)	1.777(7)
(2P1)NH2···O1(w2)	2.706(7)
(2P3)NH3···O1(w2)	2.15(3)
(1P6)NH12···O2(w2)	2.18(1)
(w2)OH1···N(2P3)	2.14(3)
(w2)OH1···O4(xyl2)	1.82(7)
(w2)OH2···O3(xyl2)	1.94(2)
(1P6)NH11···O3(xyl2)	2.31(3)
(1P4)N···OH2(xyl2)	2.25(3)
(xyl2)OH3···N(1N3)	1.87(1)
(2P3)NH4···O4(xyl2)	2.38(3)
(xyl2)OH4···N(1N3)	2.383(3)
(1N4)NH8···O5(xyl2)	1.740(1)
(2N1)NH5···O1(xyl2)	2.068(7)
(xyl2)OH1···N(2N2)	1.786(5)

[a] Atom numbers are those of Scheme S2. [b] Values in parenthesis are standard deviations in the last significant figure.

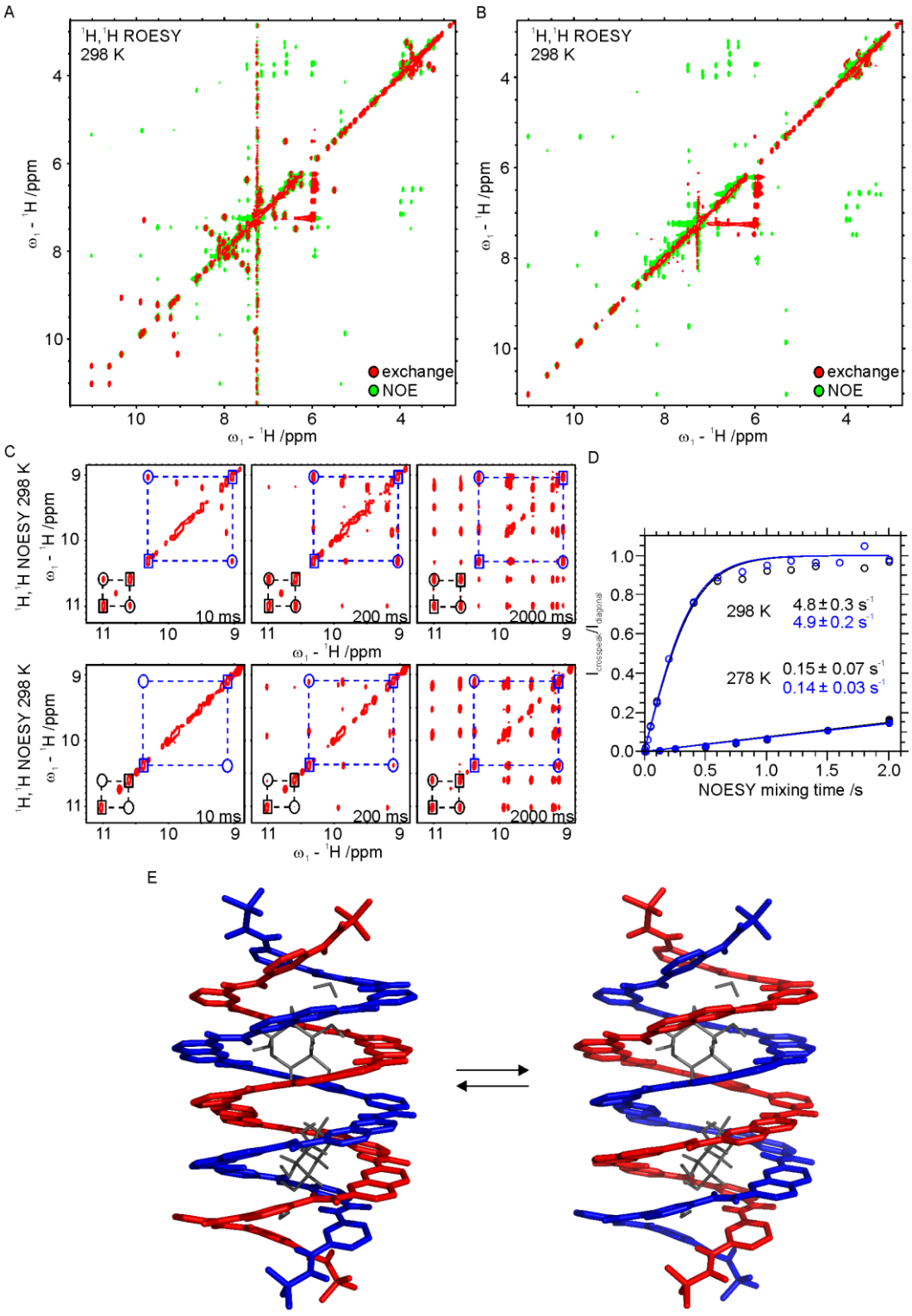

Figure S13. Exchange rate measurement for the $(\mathbf{2})_2 \supset (\text{D-}\mathbf{3})_2$ complex. (A) ^{1}H,^{1}H-ROESY spectrum of 1 mM $(\mathbf{2})_2$ with 2 mM natural abundance D-**3** in $CDCl_3$/DMSO-d_6 (95:5), measured at 298 K and a field strength of 700 MHz. Crosspeaks arising from chemical exchange are in red, and crosspeaks due to nOe have the inverse sign and are shown in green. All of the equivalent protons between the two stands of the the foldamer double helix display chemical exchange. (B) ^{1}H,^{1}H-ROESY of the same sample measured at 278 K. Note the chemical exchange is essentially absent at this lower temperature. (C) Quantitifcation of the exchange rates at 298 K (top) and 278 K (bottom) using ^{1}H,^{1}H-NOESY spectra with varying mixing times on a sample of 1 mM $(\mathbf{2})_2$ with 2 mM natural abundance D-**3** in $CDCl_3$/DMSO-d_6 (95:5), measured at 298 K and a field strength of 700 MHz. (D) Exchange rates obtained from a fit of the intensity ratio of the crosspeak versus the diagonal peak from the ^{1}H,^{1}H-NOESY spectra using the Qti plot program. (E) Rapid exchange occurs at 298 K whereby the relative positions of the two strands in the double helix interconvert. Due to the strand symmetry, the two populations are otherwise spatially identical. This is reflected by the fact that the bound xylose displays a single set of chemical shifts.

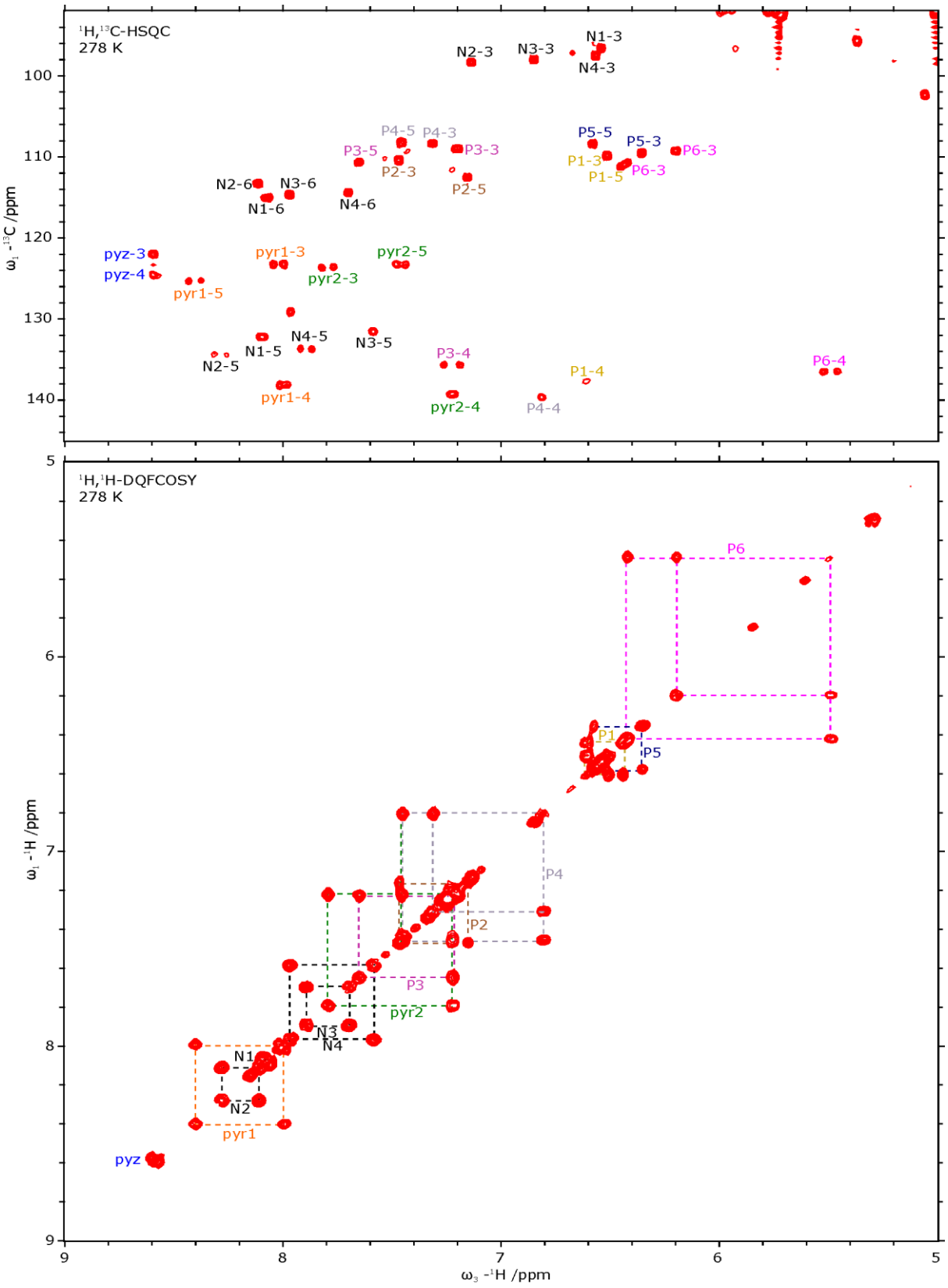

Figure S14. Aromatic ^{1}H and ^{13}C chemical shift assignment at 278 K of (**2**)$_2$ within the (**2**)$_2$ ⊃ (D-**3**)$_2$ complex. Top, aromatic region of a ^{1}H,^{13}C-HSQC spectra measured on a sample of 1 mM (**2**)$_2$ and 2 mM ^{13}C-labeled (D-**3**)$_2$ in $CDCl_3$/DMSO-d_6 (95:5) at a field strength of 700 MHz. Crosspeaks are annotated by residue name and atom number as in Scheme S2. Bottom, aromatic region of a ^{1}H,^{1}H-COSY measured on the same sample. The spin systems of the aromatic rings are connected by dashed lines and annotated by residue number. Note the the chemical shifts at 278 K have the same values as observed for the sample at 298 K (Tables S1-S3).

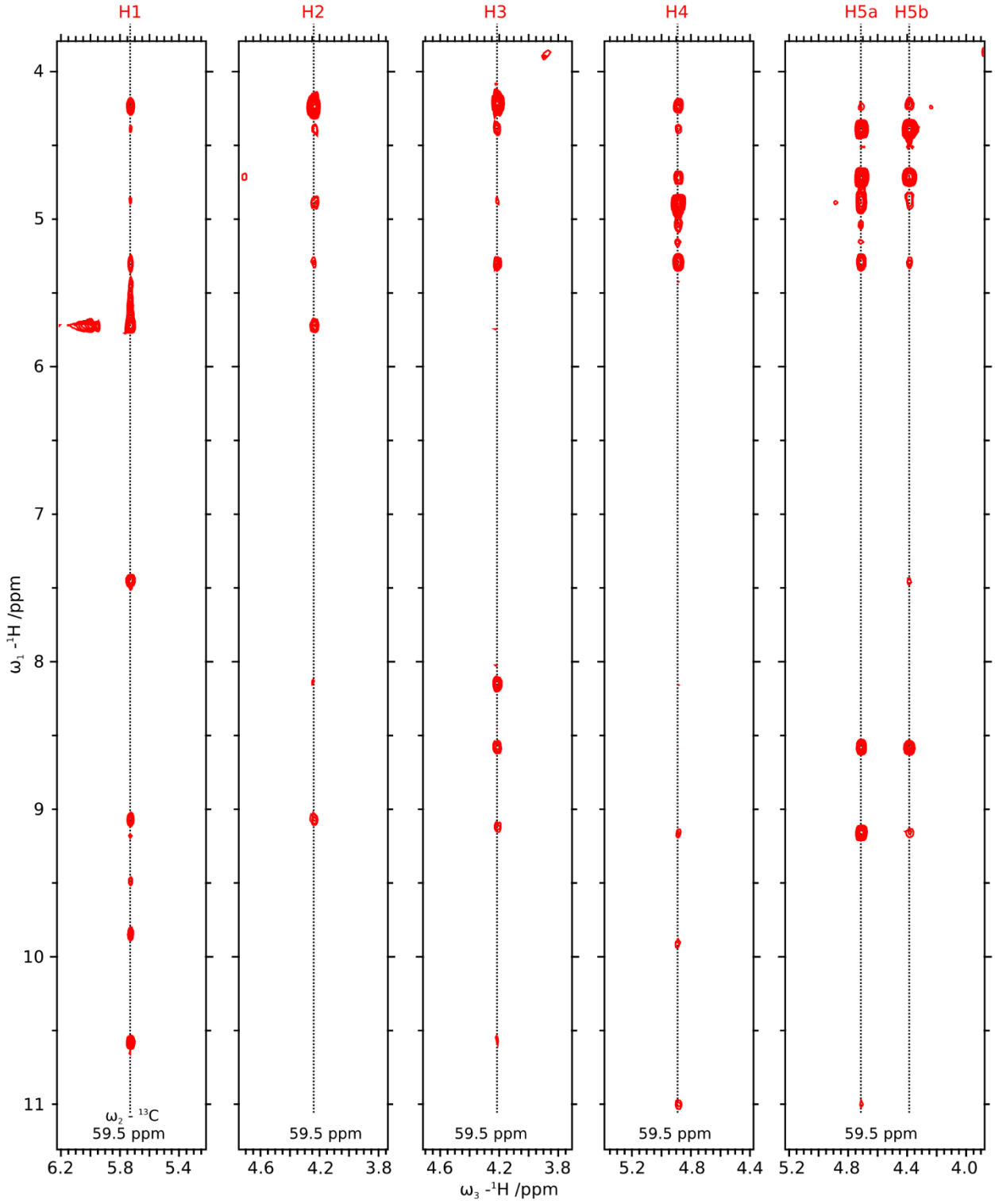

Figure S15. nOe crosspeaks involving xylose ^{13}C-bound protons in the (**2**)$_2$ ⊃ (D-**3**)$_2$ complex at 278 K. Selected 2D strips from the 3D ^{13}C-HSQC-NOESY (150 ms mixing time) measured on a sample of 1 mM (**2**)$_2$ and 2 mM ^{13}C-labeled D-**3** in $CDCl_3$/DMSO-d_6 (95:5) at a field strength of 700 MHz. The ^{13}C frequency of each strip is indicated at the bottom of each panel, and the identity of each proton of the encapsulated ^{13}C-labeled xylose is indicated at the top. Crosspeaks indicate all intramolecular and intermoleclar protons in close proximity within the the (**2**)$_2$ ⊃ (D-**3**)$_2$ complex.

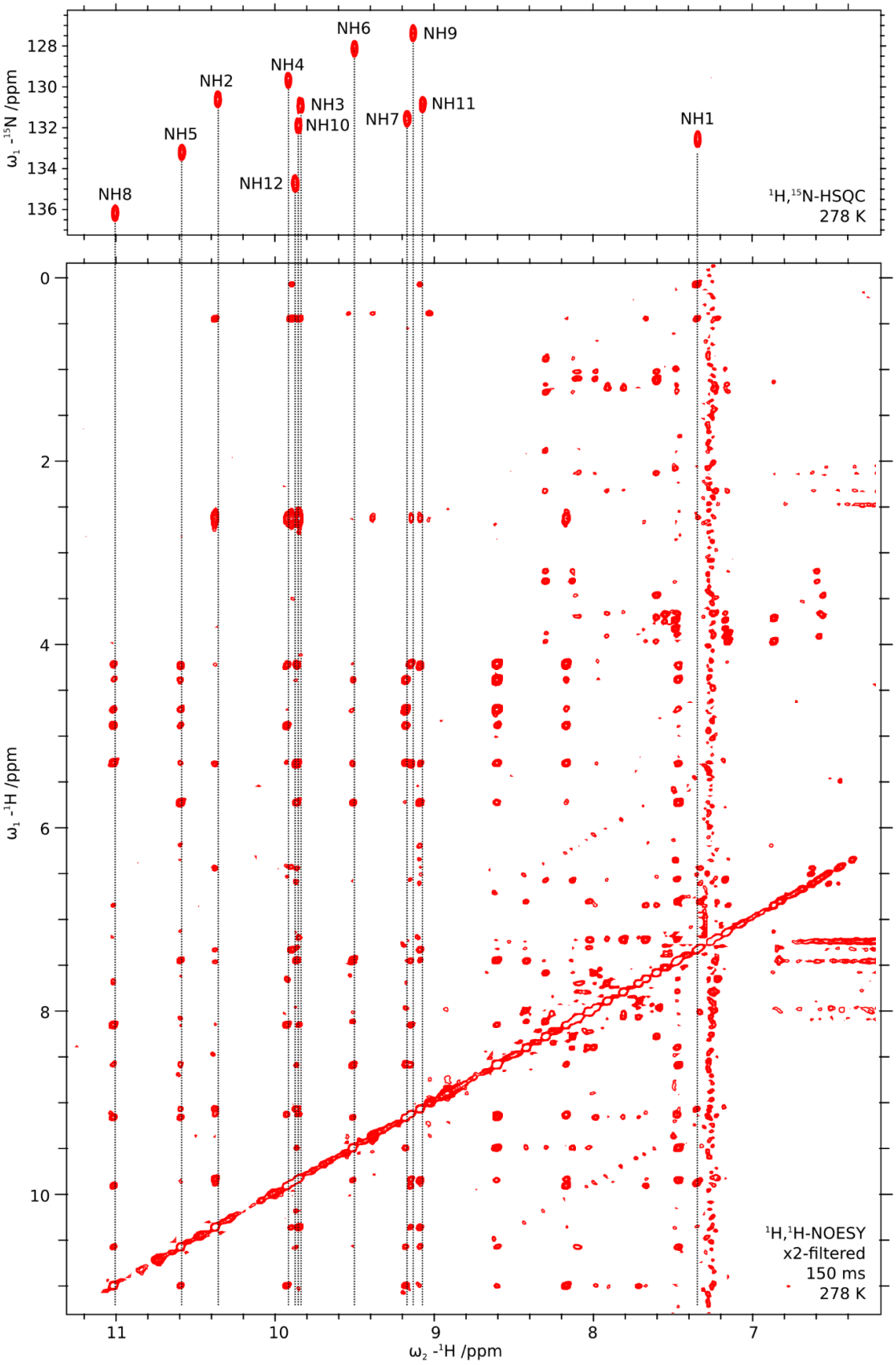

Figure S16. nOe crosspeaks involving foldamer amide protons in the $(\mathbf{2})_2 \supset (\text{D-}\mathbf{3})_2$ complex at 278 K. Top, natural abundance $^{1}H^{15}N$-HSQC measured on a sample of 1 mM $(\mathbf{2})_2$ and 2 mM ^{13}C-labeled D-**3** in $CDCl_3$/DMSO (95:5) at a field strength of 700 MHz. The amide crosspeaks are annotated as in Scheme S2. Bottom, selected region of the x2-filtered ^{1}H,^{1}H-NOESY (150 ms mixing time) on the same sample. Note that the horizontal axis (w2) is filtered to exclude all protons connected to ^{13}C nuclei, whereas the other dimension observes all protons. Crosspeaks indicate all intramolecular and intermoleclar protons in close proximity within the the $(\mathbf{2})_2 \supset (\text{D-}\mathbf{3})_2$ complex.

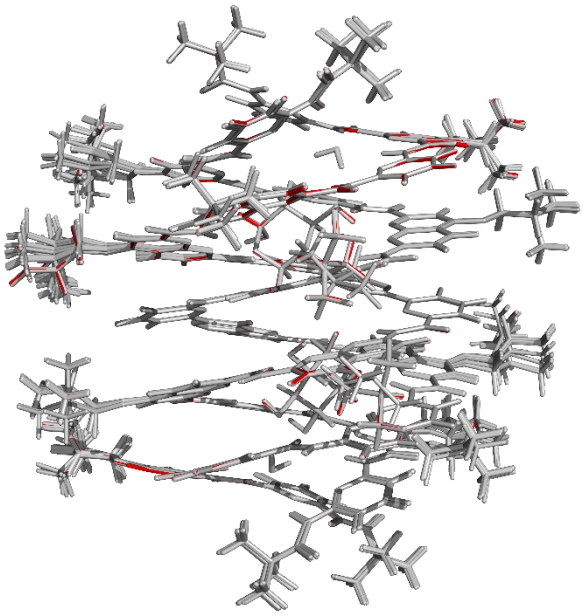

Figure S17. Superposition of the ensemble of 20 high-resolution NMR structures (grey) with the X-ray crystal structure (red).

4.2 NMR structure of the $(2)_2 \supset$ (D-3;D-4)

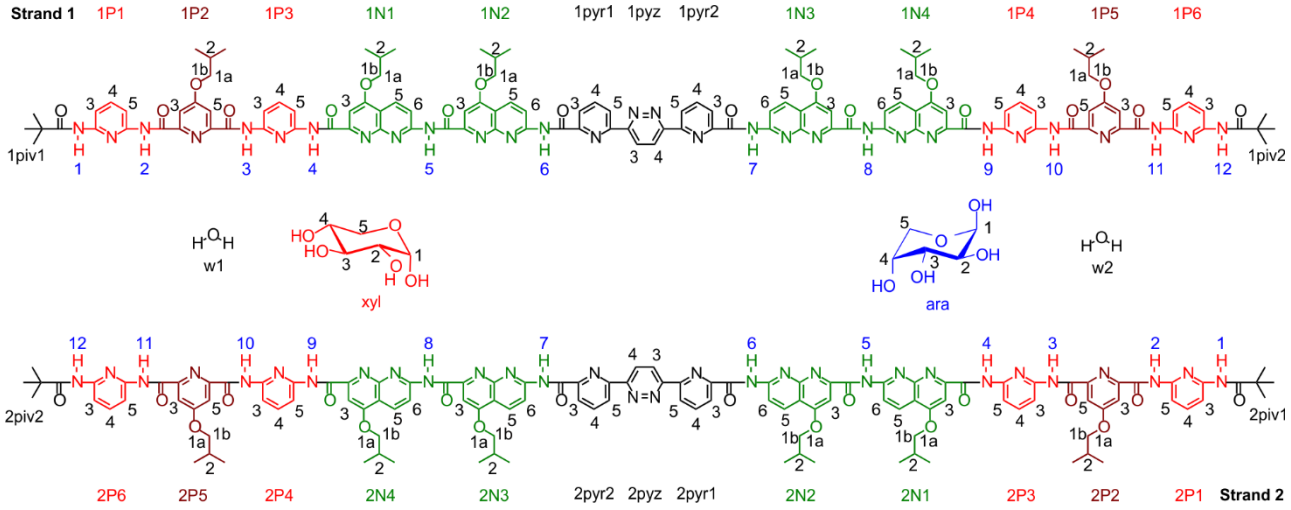

Scheme S3. Labelling of the $(2)_2 \supset$ (D-**3**;D-**4**) complex.

Table S6. Partial assignment of the ^{1}H chemical shifts of (**2**)$_2$ ⊃ (D-**3**;D-**4**) in $CDCl_3$/ DMSO-d_6 (95:5) at 298K (800MHz).

Monomer	Atom	^{1}H (ppm)	Monomer	Atom	^{1}H (ppm)
1P1	NH1	7.133	2P1	NH2	9.948
	NH2	10.235			
1P3	NH3	9.775	2P3	NH3	7.994
	NH4	10.027		NH4	9.310
1N1	NH5	10.439	2N1	NH5	10.593
1N2	NH6	9.616	2N2	NH6	10.356
1pyz	H3	8.805	2pyz	H3	8.782
	H4	9.373		H4	8.367
1N3	NH7	11.247	2N3	NH7	8.941
1N4	NH8	11.264	2N4	NH8	11.060
1P4	NH9	9.135	2P4	NH9	9.168
	NH10	8.778		NH10	9.956
1P6	NH11	8.386	2P6	NH11	9.116
				NH12	9.696
D-**3**	H1	5.923	D-**4**	H1	6.698
	H2	4.412		H2	4.081
	H3	4.262		H3	3.934
	H4	4.936		H4	3.928
	H5a	4.467		H5a	3.664
	H5b	4.816		H5b	4.360
	OH1	7.169		OH1	6.514
	OH2	5.255		OH2	7.083
	OH3	8.155		OH3	6.344
	OH4	4.456		OH4	8.404

Table S7. NMR statistics for the ensemble of fifteen structures of $(\mathbf{2})_2 \supset$ (D-**3**;D-**4**)

NMR distance restraints	
Total	54
xylose-capsule	18
arabinose-capsule	12
xylose-xylose	12
arabinose-arabinose	10
xylose-arabinose	2
Structure statistics (mean and standard deviation)	
Violations	
Distance restraints (Å)	0.002 ±0.004
Energy (kJ/mol)	16±3
Minimization Energies (kJ/mol)[a]	
Total	-941±18
Stretch	286±7
Bend	1018±5
Tortion	133±5
Improper torsion	4.1±0.3
VDW	2526±28
Electrostatic	-4581±10
Cross terms	15±2
Solvation	-297±3
rmsd between 4344 atoms pairs (Å)	
1.300	

[a] Final energies from minimization by using MMFFs (Maestro v. 6.5.007)

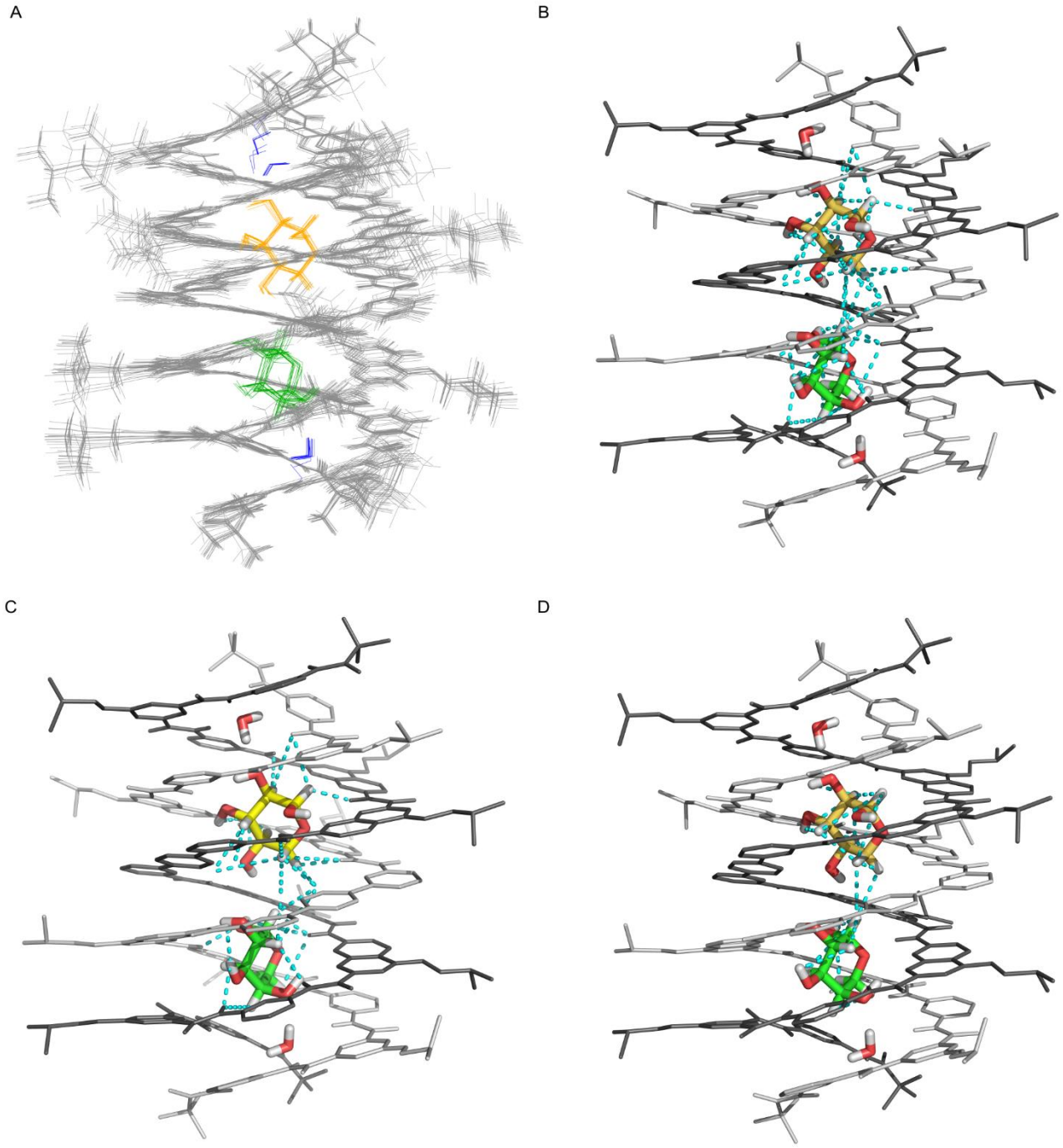

Figure S18. High-resolution NMR structure of the $(\mathbf{2})_2 \supset$ (D-**3**;D-**4**)complex. (A) ensemble of 20 structures. (B) Distance restraints used to calculate the ensemble of 20 structures. Dotted cyan lines indicate the complete set of 54 distance restraints mapped onto a representative structure from the ensemble. (C) Location of the 30 intermolecular capsule-sugar restraints used to position the guests within the capsule. (D) Location of the 12 intramolecular restraints that confirm the conformation of the encapsulated guests and of the 2 inter-sugar restraints. In all representations each strand is shown in tube representation and colored in a different tone of gray. Oxygen atoms are colored in red; carbon atoms of D-**3** and D-**4** are colored in yellow and green, respectively.

Table S8. OH···N, NH···O and OH···O hydrogen bonding distances in the $(\mathbf{2})_2 \supset$ (D-**3**, D-**4**) complex.[a]

	d **(Å)**[b]
(w1)OH2···N(1P1)	2.4(2)
(2P4)NH10···O3(xyl)	2.14(9)
(1P1)NH2···O(w1)	2.00(5)
(1P3)NH3···O(w1)	2.0(1)
(w1)OH2···N(2P6)	2.1(2)
(w1)OH1···O3(xyl)	2.6(4)
(2P6)NH11···O3(xyl)	2.2(2)
(xyl)OH2···N(2P4)	2.6(3)
(2P4)NH9···O4(xyl)	1.94(6)
(xyl)OH3···N1(2N4)	2.12(8)
(xyl)OH3···N2(2N4	2.03(3)
(1N1)NH5···O1(xyl)	2.6(2)
(xyl)OH1···N(1N2)	1.77(4)
(1N3)NH7···O5(xyl)	2.5(1)
(xyl)OH4···N(1N3)	1.91(2)
(2P1)NH2···O(w2)	2.00(3)
(2P3)NH3···O(w2)	2.1(1)
(1P6)NH12···O(w2)	2.2(1)
(w2)OH2···N(1P6)	2.30(9)
(w2)OH2···N(2P1)	2.5(2)
(w2)OH1··· O5(ara)	2.08(7)
(1P4)NH10···O4(ara)	1.89(6)
(ara)OH4···N(1N4)	2.3(1)
(1N4)NH8···O1(ara)	1.93(9)
(2N1)NH5···O2	2.08(7)
(ara)OH2···N(2N2)	1.98(2)
(ara)OH3···N(1P4)	1.995(9)
(2N2)NH6···O3(ara)	2.15(9)
(ara)OH1···N(1N3)	1.85(4)
(1P4)NH9···O5(ara)	2.0(2)
(ara)OH4···N(1N4)	2.4(1)

[a] Atom numbers are those of Scheme S3. [b] Values in parenthesis are standard deviations in the last significant figure.

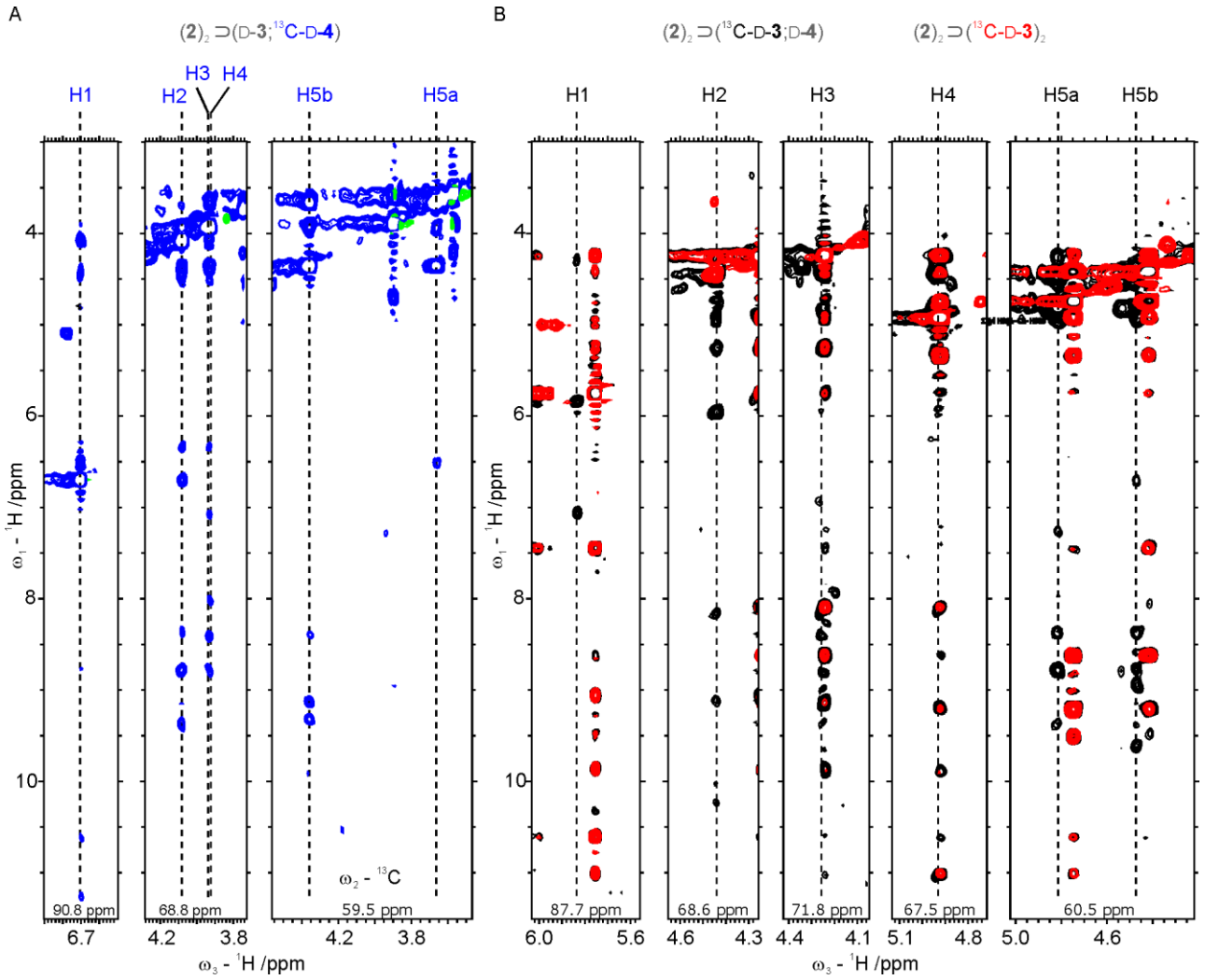

Figure S19. nOe crosspeaks involving ^{13}C-bound protons in the (**2**)$_2$ ⊃ (D-**3**, D-**4**) complex. (A) Selected 2D strips from the 3D ^{13}C-HSQC-NOESY (150 ms mixing time) measured on a sample of 1 mM (**2**)$_2$ with 1 mM natural abundance D-**3** and 1 mM ^{13}C-labeled D-**4** in $CDCl_3$/DMSO-d_6 (95:5) at a field strength of 800 MHz. The ^{13}C frequency of each strip is indicated at the bottom of each panel, and the identity of each proton of the encapsulated ^{13}C-labeled D-arabinose is indicated at the top. Crosspeaks indicate all intramolecular and intermoleclar protons in close proximity within the the (**2**)$_2$ ⊃ (D-**3**, D-**4**) complex. (B) Selected 2D strips from the 3D ^{13}C-HSQC-NOESY (150 ms mixing time), this time measured on a sample of 1 mM (**2**)$_2$ with 1 mM ^{13}C-labelled D-**3** and 1 mM natural abundance D-**4** in $CDCl_3$/DMSO (95:5) at a field strength of 800 MHz (black peaks). For comparison, the spectrum is by the 3D ^{13}C-HSQC-NOESY of the sample containing only xylose (red peaks): 1 mM (**2**)$_2$ and 2 mM ^{13}C-labeled D-**3** in $CDCl_3$/DMSO-d_6 (95:5). The crosspeaks that are similar in both samples correspond to the homomeric complex (**2**)$_2$ ⊃ (D-**3**)$_2$, whereas the black crosspeaks unique to the first spectrum belong to the heteromeric complex (**2**)$_2$ ⊃ (D-**3**, D-**4**).

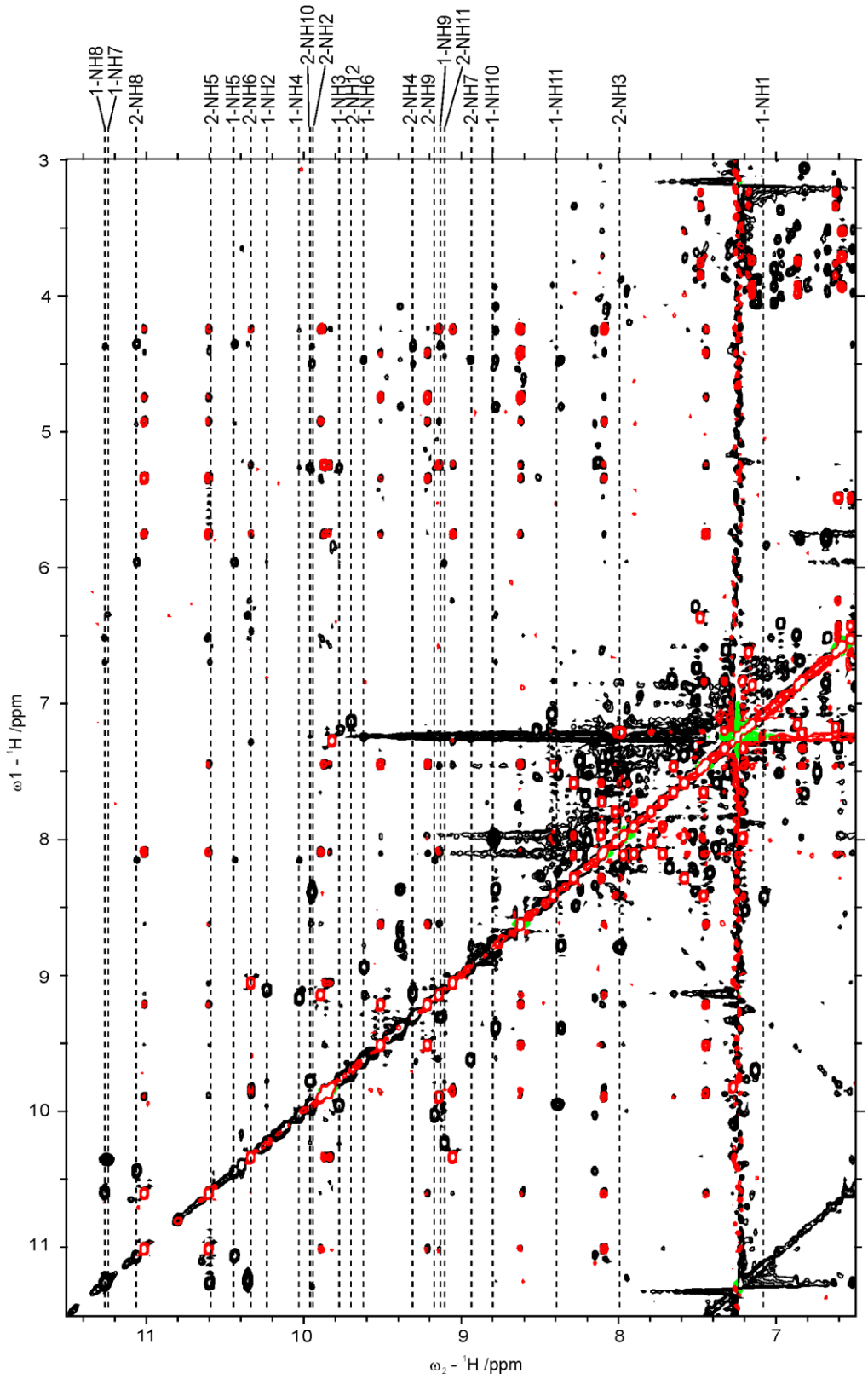

Figure S20. nOe crosspeaks involving foldamer amide protons in the $(\mathbf{2})_2 \supset$ (D-**3**, D-**4**) complex. Selected region from two x2-filtered ^{1}H,^{1}H-NOESY (150 ms mixing time) spectra. The first spectrum (in black) used a sample containing 1 mM $(\mathbf{2})_2$, 1 mM ^{13}C-labelled D-**3** and 1 mM natural abundance D-**4**, in $CDCl_3$/DMSO-d_6 (95:5) at a field strength of 800 MHz. For comparison, the second spectrum (in red) uses the sample containing only xylose: 1 mM $(\mathbf{2})_2$ and 2 mM ^{13}C-labeled D-**3** in $CDCl_3$/DMSO (95:5). Note that the horizontal axis (w2) is filtered to exclude all protons connected to ^{13}C nuclei, whereas the other dimension observes all protons. The crosspeaks that are similar in both samples correspond to the homomeric complex $(\mathbf{2})_2 \supset$ (D-**3**)$_2$, whereas the black crosspeaks unique to the first spectrum belong to the heteromeric complex $(\mathbf{2})_2 \supset$ (D-**3**, D-**4**). The foldamer double helix amides unique to the heteromeric complex $(\mathbf{2})_2 \supset$ (D-**3**, D-**4**) are indicated by dashed lines and annotated as in Scheme S3.

Figure S21. List of theoretical diastereoisomers which can form when *P/M* (**2**)$_2$ is mixed with D-xylose and D-arabinose. The list consists of 42 diastereomeric complexes. αXp and βXp stand for α-D-xylopyranose and β-D-xylopyranose, respectively. αAp, βAp, αAf and βAf stands for α-D-arabinopyranose, β-D-arabinopyranose, α-D-arabinofuranose and β-D-arabinofuranose. Note that only the 1:2 complex are considered.

5. X-Ray crystallography

5.1 X-Ray crystallographic data for 2.

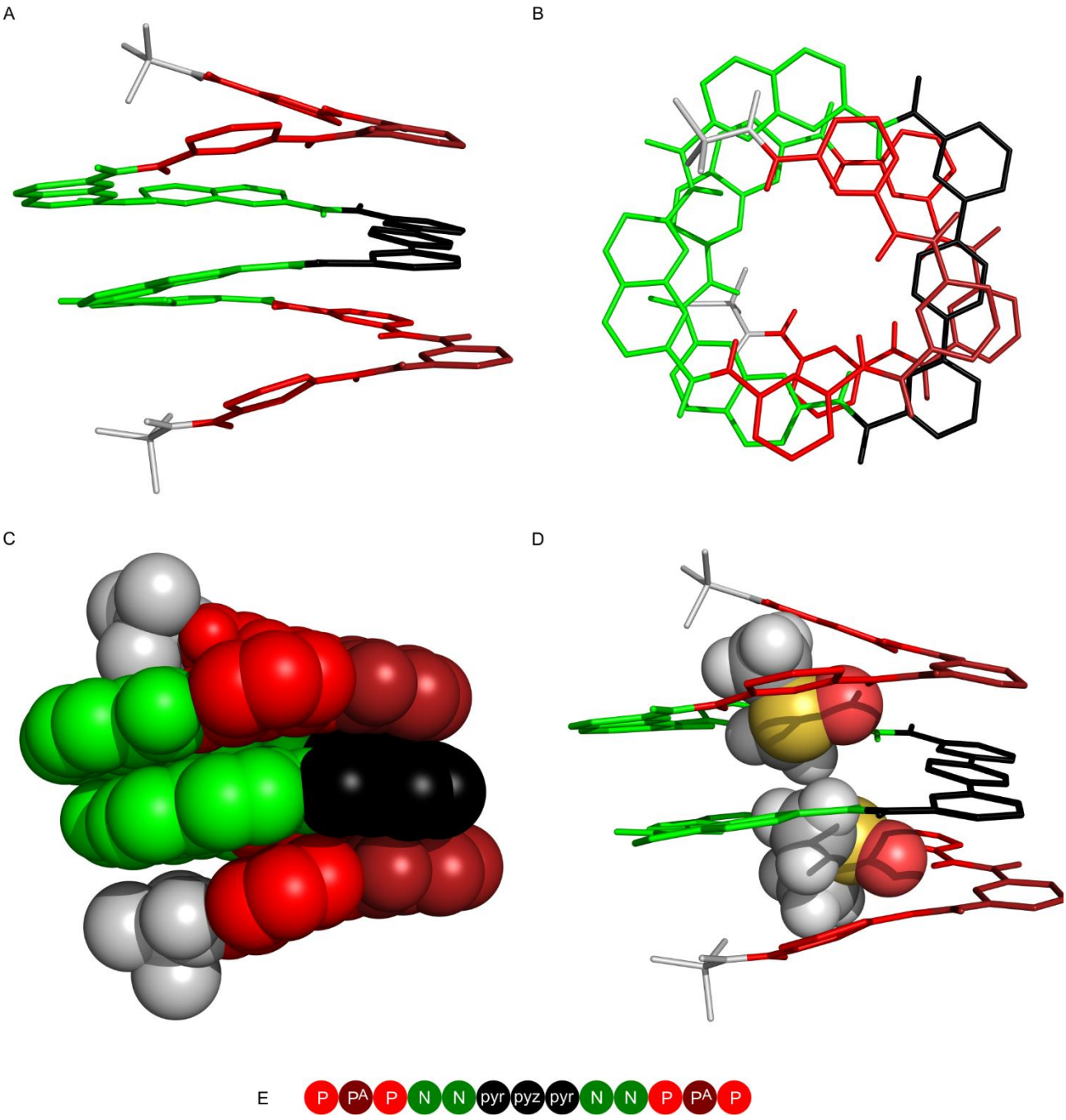

Figure S22. Solid-state structure of **2**: side (A) and top (B) views shown in tube representation; side view in CPK representation (C); side view with encapsulated solvent molecules CPK representation (D); Letter and colour codes of the amino acid, diamine, and diacid monomers (E). Isobutoxy side chains and cavity-excluded solvent molecules and counterions are omitted for clarity.

Table S9. Crystal data and refinement details for **2** ⊃ $(DMSO)_2$

Identification code	p3n2ppp_a
Crystalization solvent	DMSO
Empirical formula	$C_{134}H_{161}N_{30}O_{25}S_7$
Formula weight	2816.34
Temperature/K	566.3
Crystal system	monoclinic
Space group	$P2_1/n$
a/Å	21.8783(9)
b/Å	17.9272(7)
c/Å	41.317(3)
α/°	90
β/°	91.699(7)
γ/°	90
Volume/Å³	16197.9(15)
Z	4
ρ_{calc}*g/cm³*	1.155
μ/mm⁻¹	1.475
F(000)	5948.0
Crystal size/mm³	0.2 × 0.2 × 0.2
Radiation	CuKα (λ = 1.54184)
2Θ range for data collection/°	6.53 to 117.86
Index ranges	$-24 \leq h \leq 22$, $-19 \leq k \leq 19$, $-45 \leq l \leq 45$
Reflections collected	164489
Independent reflections	23231 [R_{int} = 0.2054, R_{sigma} = 0.2204]
Data/restraints/parameters	23231/0/1797
Goodness-of-fit on F^2	0.949
Final R indexes [I>=2σ (I)]	R_1 = 0.1321, wR_2 = 0.3222
Final R indexes [all data]	R_1 = 0.2771, wR_2 = 0.4124
Largest diff. peak/hole / e Å⁻³	0.46/-0.34
CCDC #	1967498

5.2 X-Ray crystallographic data for $(2)_2 \supset (H_2O)_{10}$

Table S10. Crystal data and refinement details for $(\mathbf{2})_2$.

Identification code	15mquan_0m
Crysalization solvent	Diffusion of hexane in $CHCl_3$
Empirical formula	$C_{120}H_{131}N_{30}O_{23}$
Formula weight	2361.54
Temperature/K	100
Crystal system	triclinic
Space group	P-1
a/Å	21.0683(14)
b/Å	21.4581(13)
c/Å	30.8205(18)
α/°	93.738(4)
β/°	97.601(4)
γ/°	92.328(4)
Volume/Å^3	13764.6(15)
Z	4
ρ_{calc}g/cm^3	1.140
μ/mm^{-1}	0.644
F(000)	4980.0
Crystal size/mm^3	0.1 × 0.1 × 0.08
Radiation	CuKα (λ = 1.54178)
2Θ range for data collection/°	4.236 to 101.106
Index ranges	$-20 \leq h \leq 21$, $-21 \leq k \leq 15$, $-30 \leq l \leq 29$
Reflections collected	90366
Independent reflections	25996 [R_{int} = 0.0805, R_{sigma} = 0.1069]
Data/restraints/parameters	25996/173/3157
Goodness-of-fit on F^2	1.542
Final R indexes [I>=2σ (I)]	R_1 = 0.1559, wR_2 = 0.3924
Final R indexes [all data]	R_1 = 0.2273, wR_2 = 0.4453
Largest diff. peak/hole / e Å^{-3}	1.43/-0.50
CCDC #	1967492

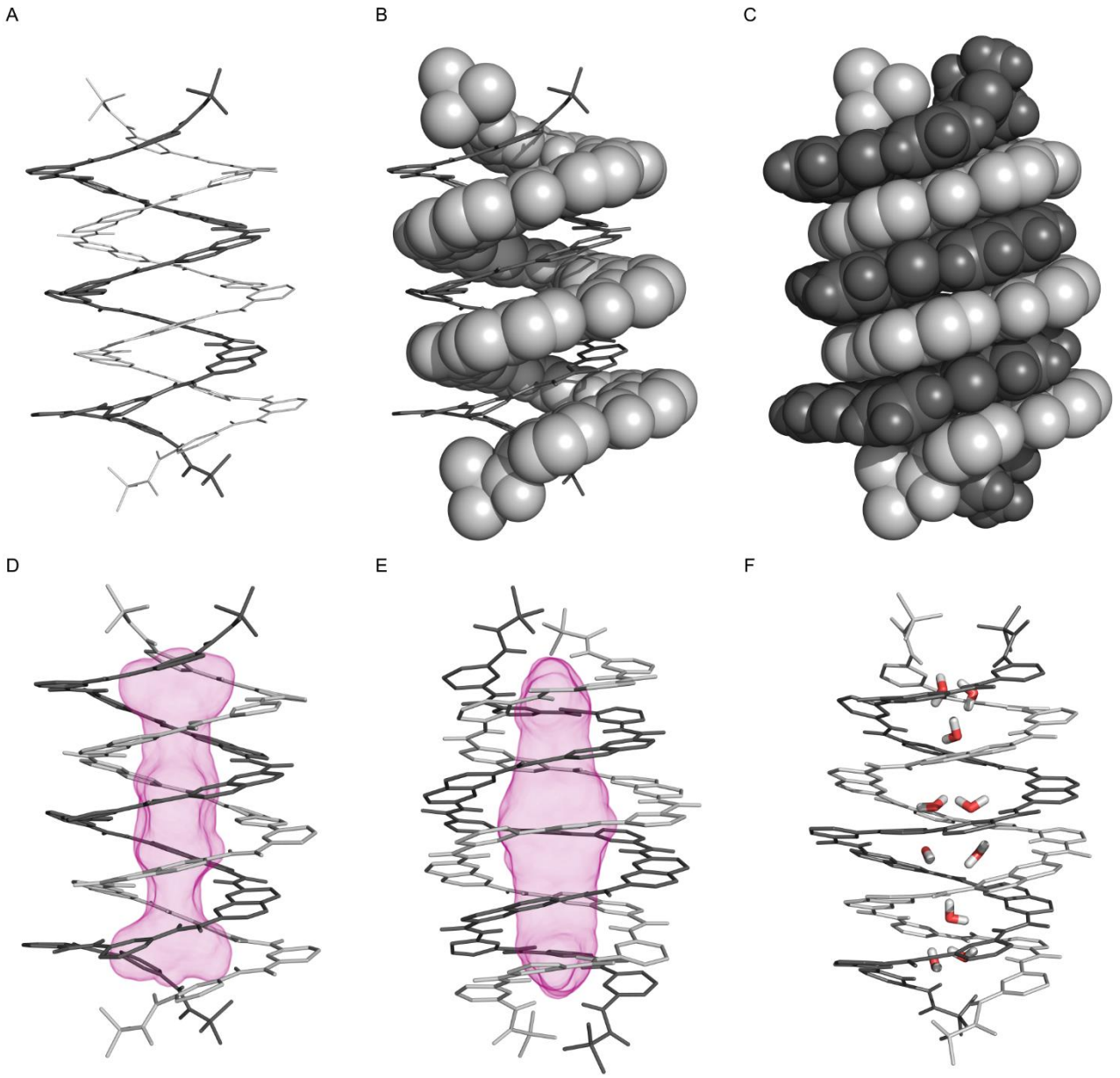

Figure S23. Solid-state structure of $(\mathbf{2})_2$. Side views shown: in tube representation (A); with one strand shown in CPK representation and the other in tube representation (B); in CPK representation (C). Side views shown in tube representation where the cavity volume of 280 $Å^3$ is shown as a transparent pink isosurface (D, E). Side view with encapsulated solvent molecules (F). In all representations each strand is colored in a different tone of gray. Side chains were omitted for clarity.

5.3 X-Ray crystallographic data for the (**2**)$_2$ ⊃ (D-**3**)$_2$

Table S11. Crystal data and refinement details for the (**2**)$_2$ ⊃ (D-**3**)$_2$ complex.

Identification code	shelxt_a
Crysalization solvent	Diffusion of hexane in $CHCl_3$/chlorobenzene/DMSO (89:10:1 vol/vol/vol)
Empirical formula	$C_{536}H_{564}Cl_6N_{120}O_{98}$
Formula weight	10467.74
Temperature/K	100
Crystal system	monoclinic
Space group	P2/c
a/Å	21.7412(3)
b/Å	35.0462(4)
c/Å	39.2898(5)
α/°	90
β/°	94.9330(10)
γ/°	90
Volume/Å^3	29825.8(7)
Z	2
ρ_{calc}g/cm^3	1.166
μ/mm^{-1}	0.916
F(000)	11012.0
Crystal size/mm^3	0.1 × 0.1 × 0.1
Radiation	CuKα (λ = 1.54184)
2Θ range for data collection/°	3.384 to 109.414
Index ranges	-22 ≤ h ≤ 22, -36 ≤ k ≤ 36, -41 ≤ l ≤ 41
Reflections collected	129058
Independent reflections	36674 [R_{int} = 0.0359, R_{sigma} = 0.0262]
Data/restraints/parameters	36674/139/3474
Goodness-of-fit on F^2	1.482
Final R indexes [I>=2σ (I)]	R_1 = 0.1132, wR_2 = 0.3287
Final R indexes [all data]	R_1 = 0.1233, wR_2 = 0.3425
Largest diff. peak/hole / e Å^{-3}	1.33/-0.89
CCDC #	1967491

6. ^{1}H NMR and ^{13}C NMR spectra of new synthetic compounds

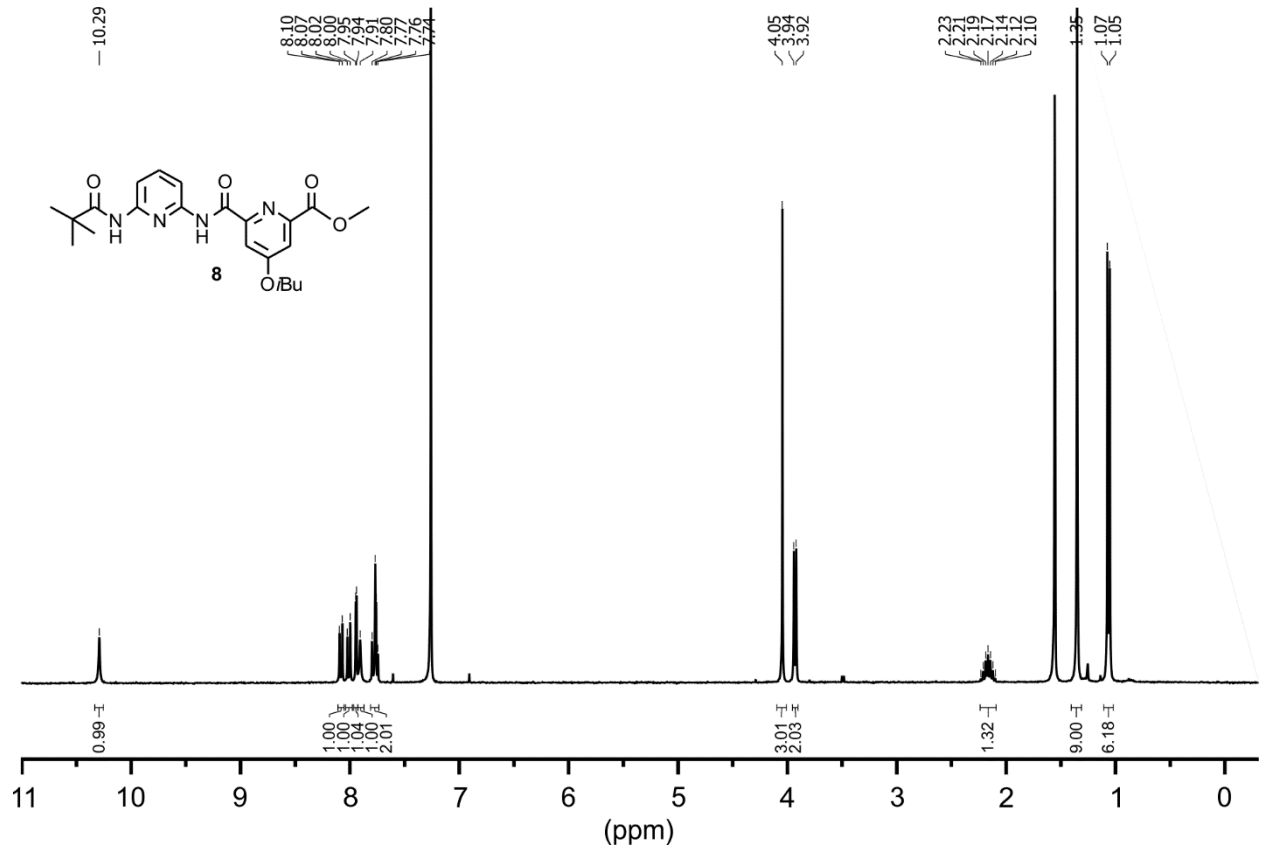

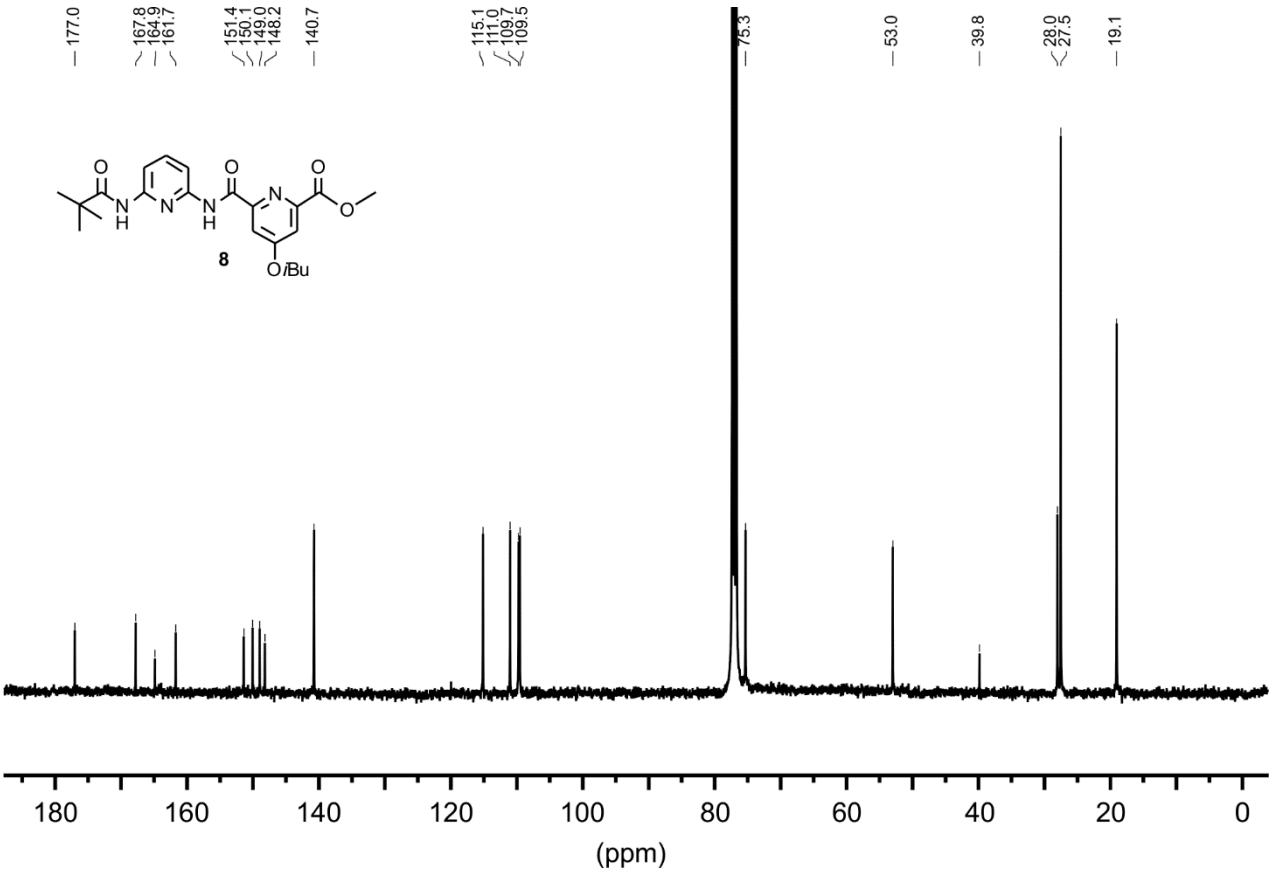

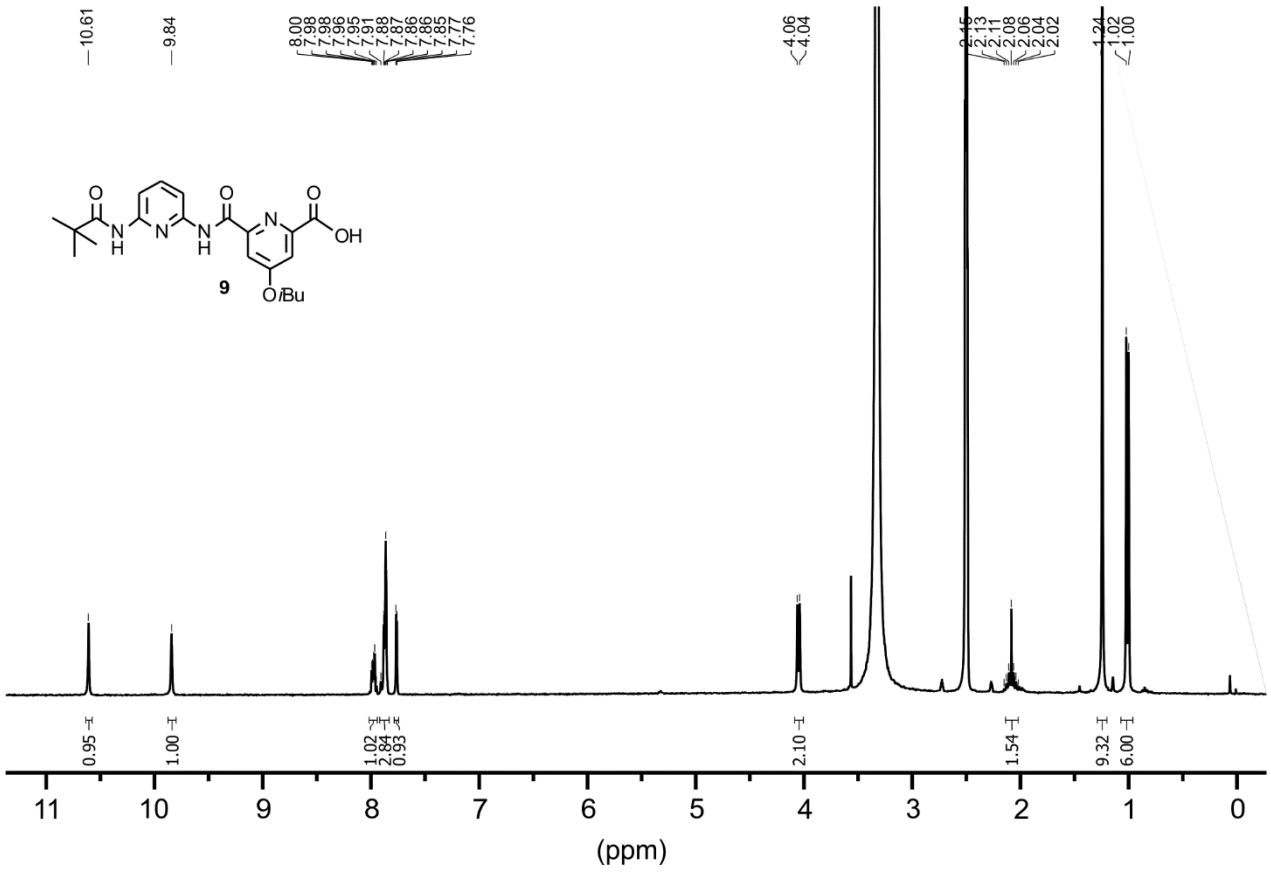
10.61
9.84
8.00
7.98
7.98
7.96
7.95
7.91
7.88
7.87
7.86
7.86
7.85
7.77
7.76
4.06
4.04
2.15
2.13
2.11
2.08
2.06
2.04
2.02
1.24
1.02
1.00
9
OiBu
0.95
1.00
1.02
2.84
0.93
2.10
1.54
9.32
6.00
(ppm)

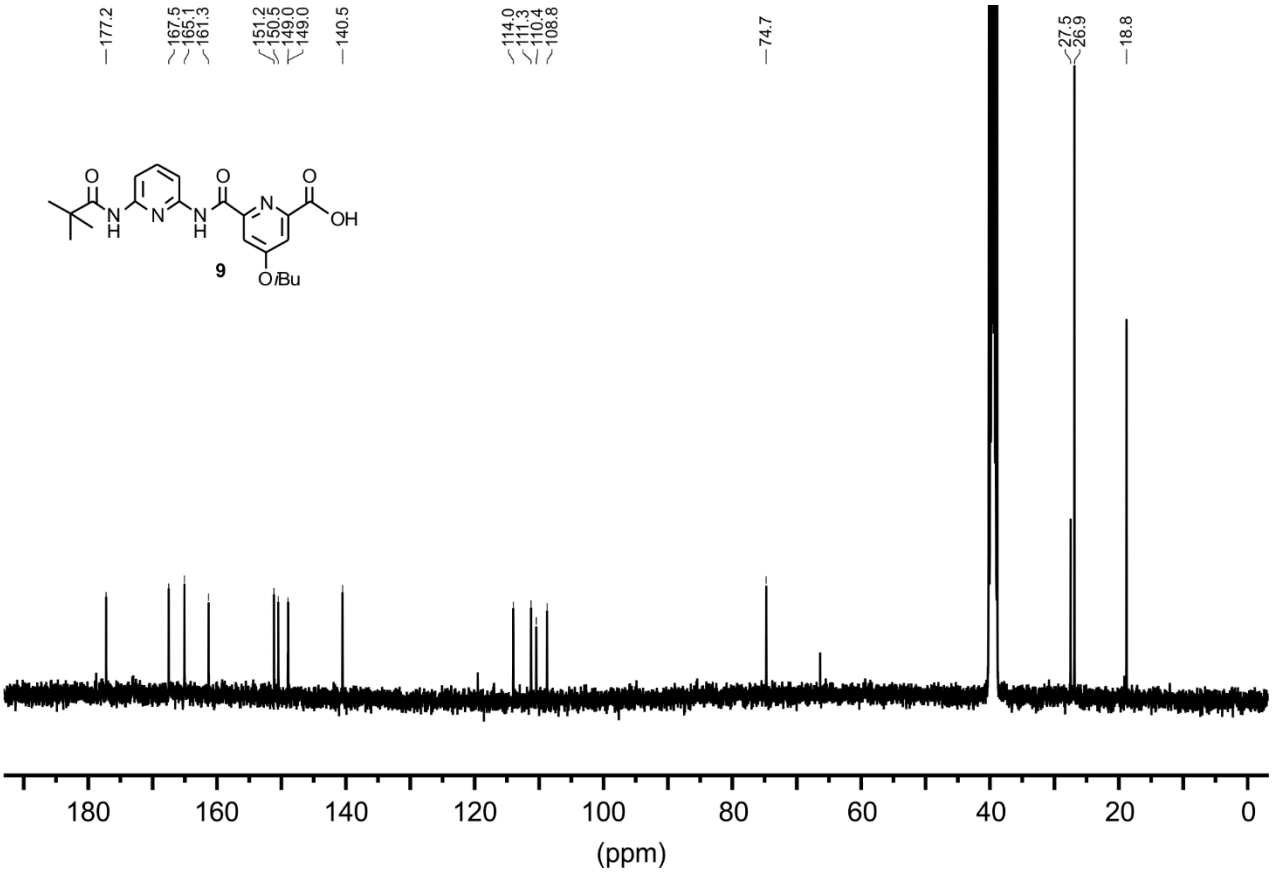
177.2
167.5
165.1
161.3
151.2
150.5
149.0
149.0
140.5
114.0
111.3
110.4
108.8
74.7
27.5
26.9
18.8
9
OiBu
(ppm)

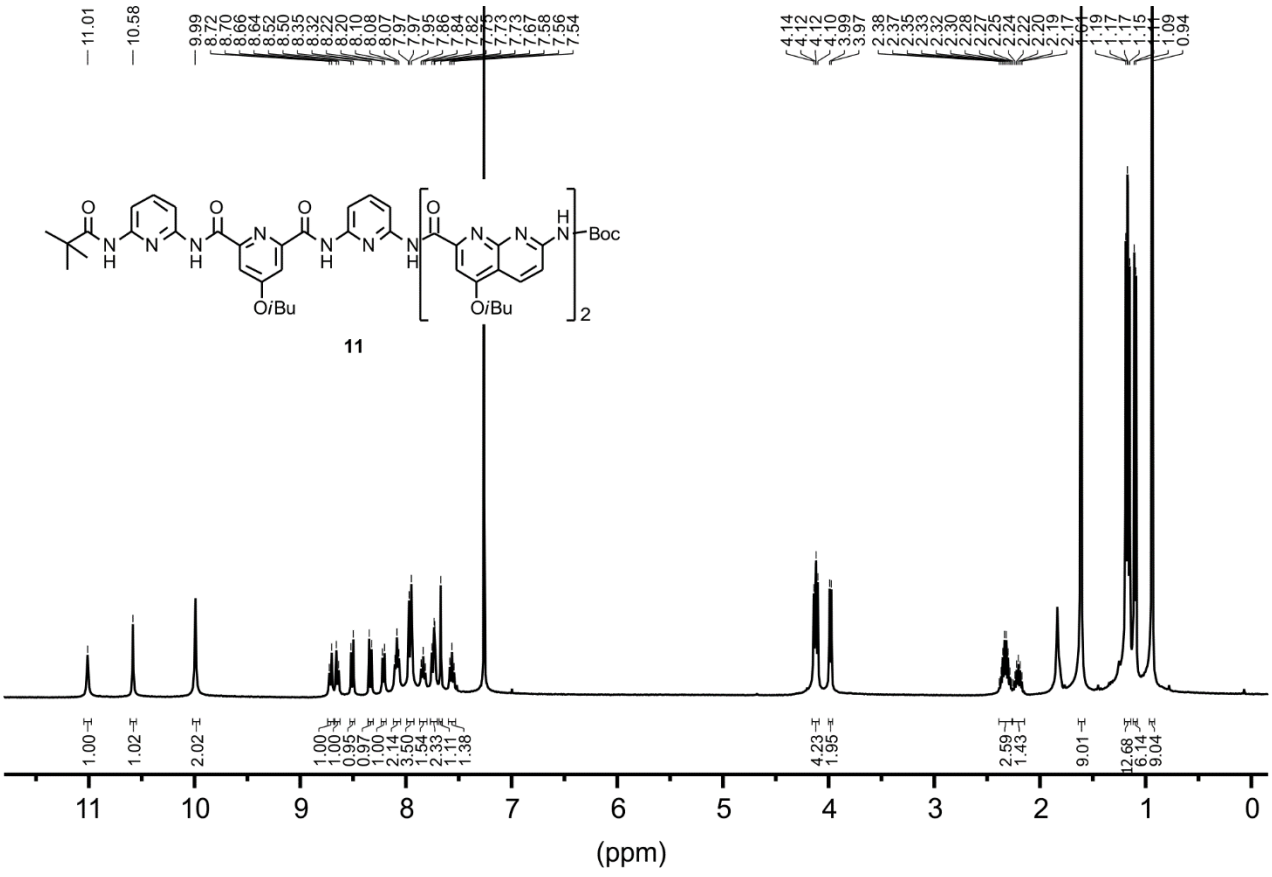
11.01
10.58
9.99
8.72
8.70
8.66
8.64
8.52
8.50
8.35
8.32
8.22
8.20
8.10
8.08
8.07
7.97
7.95
7.86
7.84
7.75
7.73
7.67
7.58
7.56
7.54
4.14
4.12
4.12
4.10
3.99
3.97
2.38
2.37
2.35
2.33
2.32
2.30
2.28
2.27
2.25
2.24
2.22
2.20
2.19
2.17
1.61
1.19
1.17
1.17
1.15
1.11
1.09
0.94
1.00
1.02
2.02
1.00
1.00
0.95
0.97
1.00
2.14
3.50
1.54
2.33
1.11
1.38
4.23
1.95
2.59
1.43
9.01
12.68
6.14
9.04
11
10
9
8
7
6
5
4
3
2
1
0
(ppm)
O/Bu
O/Bu
Boc
2
11

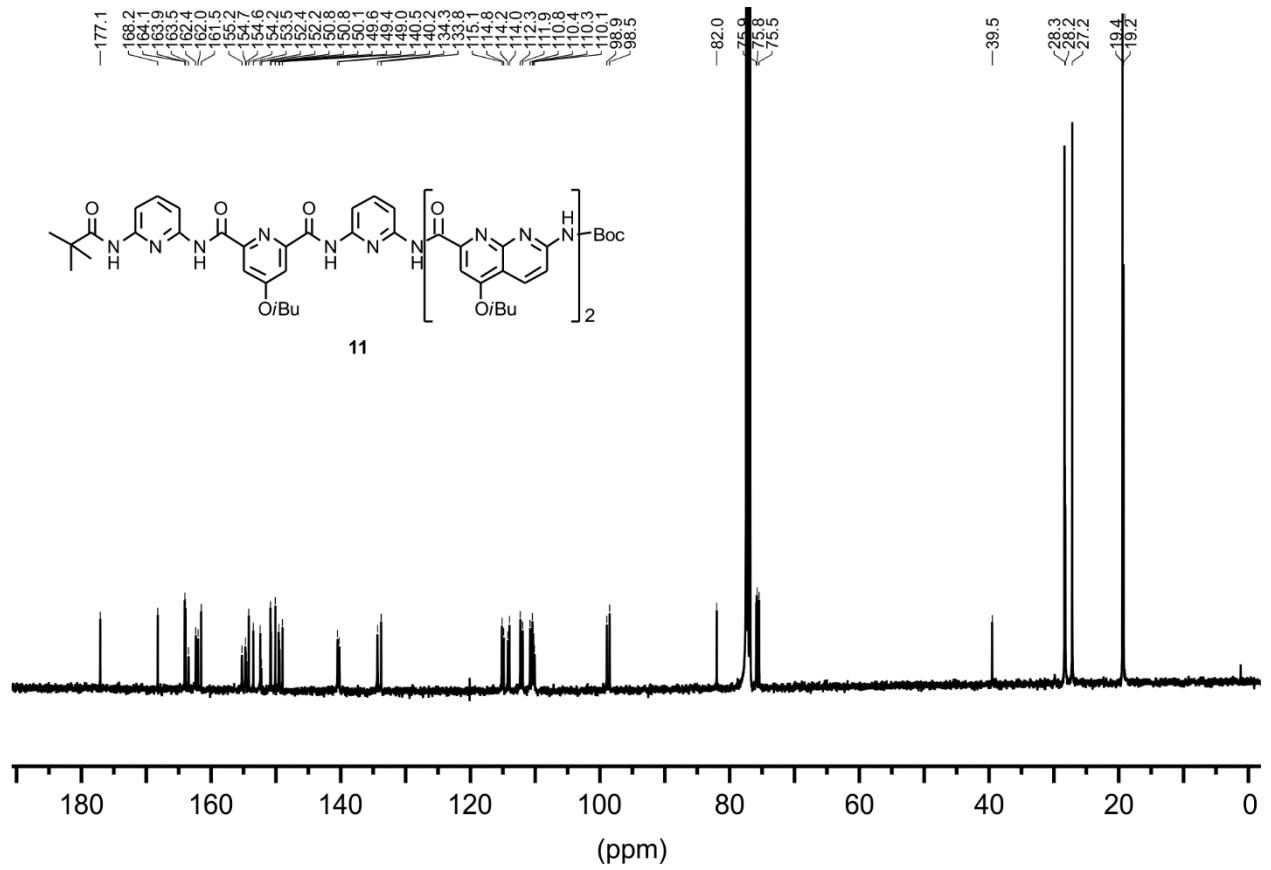
177.1
168.2
164.1
163.9
163.5
162.4
162.0
161.5
155.2
154.7
154.6
154.2
153.5
152.4
152.2
150.8
150.8
150.1
149.6
149.4
149.0
140.5
140.2
134.3
133.8
115.1
114.8
114.2
114.0
112.3
111.9
110.8
110.4
110.3
110.1
98.9
98.5
82.0
75.9
75.8
75.5
39.5
28.3
28.2
27.2
19.4
19.2
180
160
140
120
100
80
60
40
20
0
(ppm)
O/Bu
O/Bu
Boc
2
11

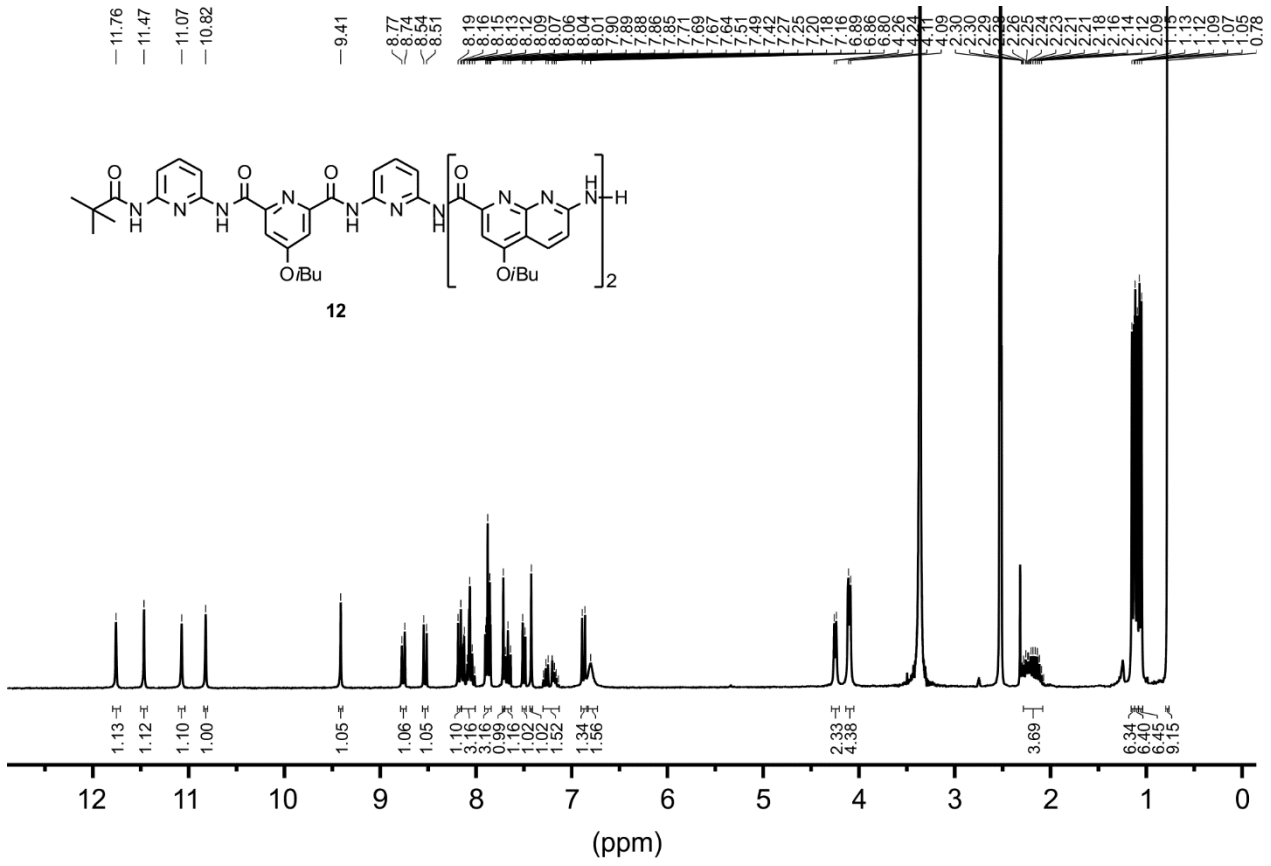
11.76
11.47
11.07
10.82
9.41
8.77
8.74
8.54
8.51
O/Bu
O/Bu
12
(ppm)

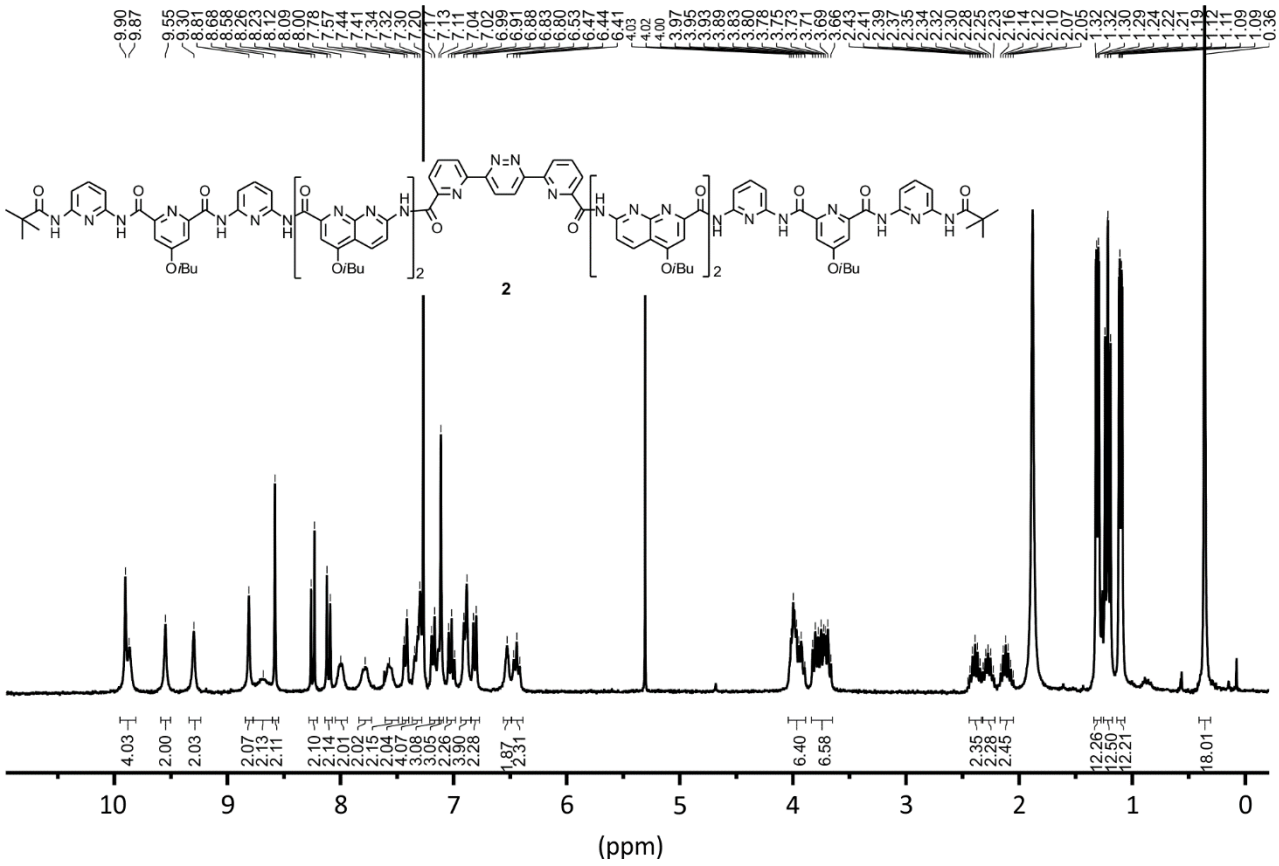
9.90
9.87
9.55
9.30
O/Bu
O/Bu
O/Bu
O/Bu
2
(ppm)

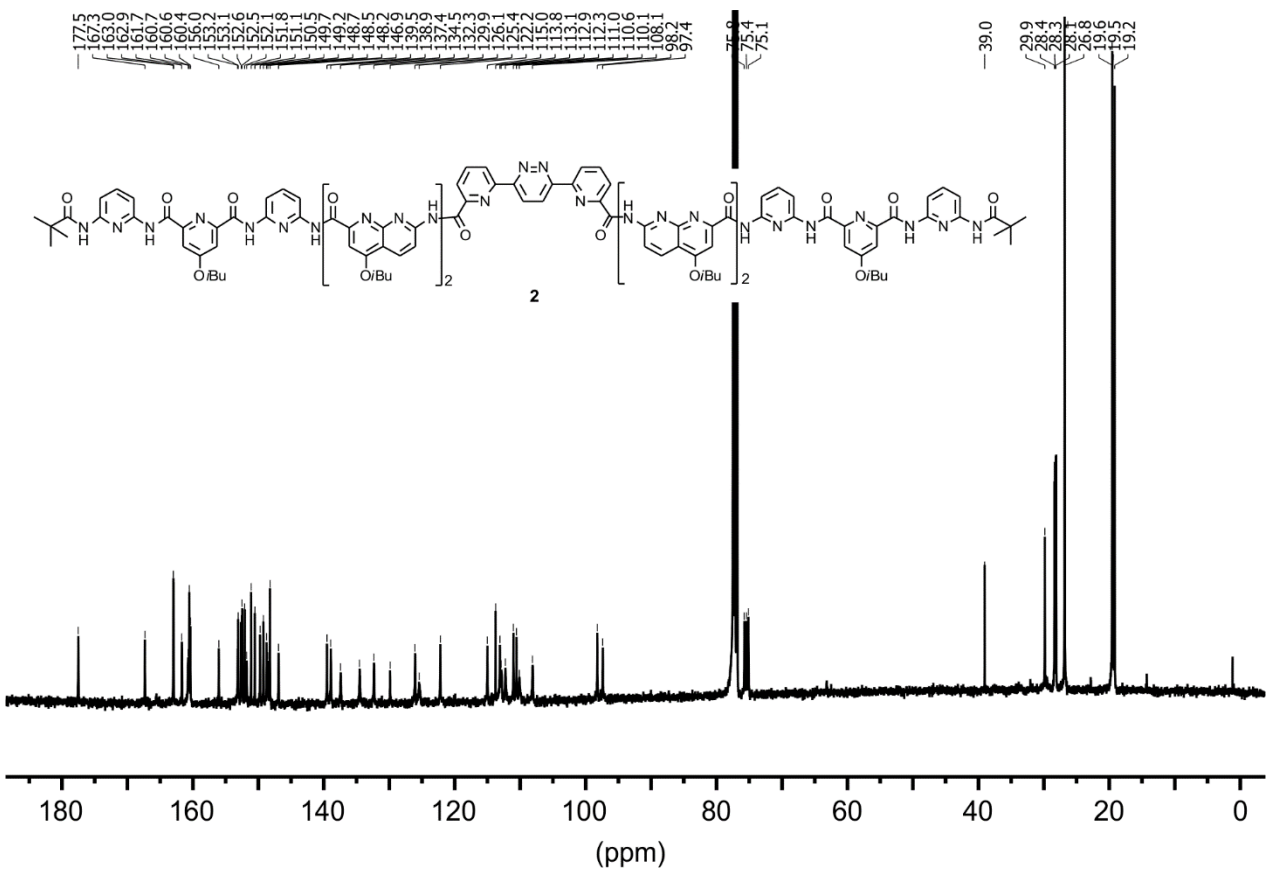
177.5
167.3
163.0
162.9
161.7
160.7
160.6
160.4
156.0
153.2
153.1
152.6
152.5
152.1
151.8
151.1
150.5
149.7
149.2
148.7
148.5
148.2
146.9
139.5
138.9
137.4
134.5
132.3
129.9
126.1
125.4
122.2
122.0
115.0
113.8
113.1
112.9
112.3
111.0
110.6
110.1
108.1
98.2
97.4
75.9
75.4
75.1
39.0
29.9
28.4
28.3
28.1
26.8
19.6
19.5
19.2
O/Bu
2
180
160
140
120
100
80
60
40
20
0
(ppm)

7. References

1. P. Gans, A. Sabatini, A. Vacca, *Ann. Chim*. **1999**, *89*, 45.
2. CrysAlisPRO : CrysAlisPRO, Oxford Diffraction /Agilent Technologies UK Ltd, Yarnton, England.
3. G. M. Sheldrick, *Acta Cryst*. **2015**, *A71*, 3
4. OLEX2: O. V. Dolomanov, L. J. Bourhis, R. J. Gildea, J. A. K. Howard and H. Puschmann. *J. Appl. Cryst.* **2009**, 42, 339-341.
5. Spek, A. L. *Acta Cryst.* **2009**, D65, 148.
6. R. A. Laskowski, *J. Mol. Graphics* **1995**, *13*, 323.
7. B. Baptiste, J. Zhu, D. Haldar, B. Kauffmann, J-M. Léger, I. Huc *Chem. Asian* J. **2010**, *5*, 1364.
8. A. B. Eldrup, C. Christensen, G. Haaima, P. E. Nielsen, *J. Am. Chem. Soc.* **2002**, *124*, 3254-3262.
9. Y. Ferrand, A. M. Kendhale, B. Kauffmann, A. Grélard, C. Marie, V. Blot, M. Pipelier, D. Dubreuil, I. Huc, *J. Am. Chem. Soc.* **2010**, *132*, 7858.